Hybridizable discontinuous Galerkin method for the two-dimensional frequency-domain elastic wave equations

Marie Bonnasse-Gahot, Henri Calandra, Julien Diaz, Stéphane Lanteri

submitted to *Geophys. J. Int.*

Hybridizable discontinuous Galerkin method for the two-dimensional frequency-domain elastic wave equations

Marie Bonnasse-Gahot[1,2], Henri Calandra[3], Julien Diaz[1], and Stéphane Lanteri[2]

[1] *Magique 3D project-team, Inria Bordeaux - Sud-Ouest, France*

[2] *Nachos project-team, Inria Sophia Antipolis - Méditerranée, France*

[3] *TOTAL Exploration & Production, Houston, Texas, USA*

SUMMARY

Discontinuous Galerkin (DG) methods are nowadays actively studied and increasingly exploited for the simulation of large-scale time-domain (i.e. unsteady) seismic wave propagation problems. Although theoretically applicable to frequency-domain problems as well, their use in this context has been hampered by the potentially large number of coupled unknowns they incur, especially in the three-dimensional case, as compared to classical continuous finite element methods. In this paper, we address this issue in the framework of so-called hybridizable discontinuous Galerkin (HDG) formulations. As a first step, we study a HDG method for the resolution of the frequency-domain elastic wave equations in the two-dimensional case. We describe the weak formulation of the method and provide some implementation details. The proposed HDG method is assessed numerically including a comparison with a classical upwind flux-based DG method, showing better overall computational efficiency as a result of the drastic reduction of the number of globally coupled unknowns in the resulting discrete HDG system.

Key words: Seismic imaging, forward problem, elastodynamic equations, frequency-domain, elastic waves, hybridizable DG method.

1 INTRODUCTION

Discontinuous Galerkin (DG) methods have been introduced in 1973 by Reed and Hill (Reed & Hill 1973). They have been increasingly studied during the last 20 years for the resolution of differential models of linear wave propagation problems, particularly in the time-domain where they proved to be accurate and efficient when they are combined with explicit time integration schemes. DG methods present a lot of advantages such as a high flexibility with regards to the mesh used for discretizing complex geometrical features, hp-adaptivity (i.e. local adaptation of the discretization parameter and interpolation degree) and easy parallelization. Without being exhaustive, we refer the reader to (Cockburn, Karniadakis, & Shu 2000), (Rivière 2008), (Hesthaven & Warburton 2007) and (Di Pietro & Ern 2011) for a detailed overview of Discontinuous Galerkin methods.

In (Grote, Schneebeli, & Schötzau 2006) and (Grote & Schötzau 2009), Grote *et al.* propose to use the Interior Penalty Discontinuous Galerkin (IPDG) (Arnold, *et al.* 2000) method for solving the second order formulation of the wave equation, and further extend the technique to Maxwell equations in (Grote, Schneebeli, & Schötzau 2008). The IPDG method has been employed in a geophysical context in (Baldassari *et al.* 2012). Many works have been devoted to the development of DG methods for the resolution of the first order formulation of the elastodynamic equations for seismic applications. In (Delcourte, Fezoui, & Glinsky-Olivier 2009), a centered flux method for the elastodynamic equations is developed, based on the works of (Fezoui *et al.* 2005) and (Piperno, Remaki, & Fezoui 2002). Moreover, adaptive variants applied to geophysical applications have been considered in (Etienne *et al.* 2010) and (Tago *et al.* 2013). Another very popular approach in seismology, the ADER method, is based on upwind fluxes and high order interpolation in space and time (Dumbser & Käser 2006)-(Dumbser, Käser, & Toro 2007)-(Käser & Dumbser 2006).

When applied to steady-state and time-harmonic problems, the main drawback of classical DG methods is their computational cost (CPU time and memory occupancy) as compared to classical (continuous) finite element (CG) methods because they incur additional degrees of freedom, especially when an arbitrarily high order interpolation of the field components is used. This is due to the fact that the degrees of freedom are local to an element and so, the degrees of freedom placed at element interfaces have to be duplicated. As a consequence, DG methods lead to larger (sparse) linear systems of equations with a higher number of globally coupled degrees of freedom as compared to CG methods on a given mesh. This explains why many authors have considered CG methods rather than DG methods to solve Helmholtz type equations, in particular in elastodynamics (see for instance (Marfurt 1984) and (Min *et al.* 2003)). Recent works have however been devoted to the application of DG methods for seismic imaging in order to take advantage of the flexibility of the discontinu-

ous formulation setting (Brossier *et al.* 2010). Note that, because of the high computational cost, this development has been limited to the numerical treatment of acoustic wave propagation.

To get around this drawback, we consider here an alternative DG method: the hybridizable DG method (HDG). The basic principle of an HDG method is to introduce a Lagrange multiplier (so-called hybrid unknown) representing the trace of a certain physical quantity on each face of the mesh elements (cells). This hybrid unknown is used to obtain the physical field unknowns defined at the element level (i.e. the usual DG degrees of freedom) thanks to purely local calculations. This approach allows to reduce drastically the number of globally coupled unknowns and thus the number of degrees of freedom of the global linear system to be solved. More precisely, the size of the matrix to be inverted only depends on the number of degrees of freedom of each face and on the number of faces of the mesh. It is worth noting that for a classical DG method, this size depends on the number of degrees of freedom of each element and on the number of elements of the mesh. Once this (interface) linear system is solved for the hybrid variable degrees of freedom, the physical field values in each element are recovered thanks to independent calculations. Moreover, the parallelization of the HDG formulation does not induce any additional difficulty in comparison with classical DG methods. We refer to (Kirby, Sherwin, & Cockburn 2012) for a comparison between CG, DG and HDG methods.

The HDG method has been introduced in (Cockburn, Gopalakrishnan, & Lazarov 2009) for a second order elliptic problem. Then, it has been developed and applied to many problems such as the frequency-domain Maxwell equations (Lanteri, Li, & Perrussel 2013)-(Nguyen, Peraire, & Cockburn 2011b), convection-diffusion problems (Nguyen, Peraire, & Cockburn 2009a)-(Nguyen, Peraire, & Cockburn 2009b) or fluid flow problems (Nguyen & Peraire 2012).

In (Nguyen, Peraire, & Cockburn 2011a), the authors propose a HDG method for the discretization of the time-domain elastodynamic equations coupled with an implicit time integration. The HDG method considered here is inspired from this work. Nevertheless, to the best of our knowledge, there is no similar work for the solution of the frequency-domain elastodynamic equations.

More recently, (Terrana, Vilotte, & Guillot 2015) consider the system of coupled elasto-acoustic equations formulated as a domain decomposition problem. The concept of Dirichlet-to-Neumann (DtN) operator is used for the definition of appropriate transmission conditions at the interface between the fluid and solid domains in this domain decomposition framework. The velocity is assumed to be single-valued on the non-overlapping interface between the fluid and solid domains, and the required transmission condition corresponds to the weak continuity of the traces of the normal forces. Then, by exploiting the Rankine-Hugoniot conditions and the solutions of appropriately defined Riemann problems in each domain, the authors obtain a definition of the numerical traces at the interface

between the fluid and solid domains. Finally, a HDG method is formulated for the elasto-acoustic coupling by defining numerical traces in terms of the DtN operators.

The rest of the paper is organized as follows. In section 2, we present the boundary value problem that we consider and the notations that we adopt for the sequel. The formulation of the HDG method is the subject of section 3. Section 4 is dedicated to numerical results, where we study the convergence of HDG and compare its performance with the ones of IPDG and CG. In appendix A, we discuss the relation between HDG and a classical nodal DG method and in appendix B we detail the discretization and the implementation of the method. The algorithm we used are described in appendix C.

2 FREQUENCY-DOMAIN ELASTIC WAVE EQUATIONS

We consider the first order formulation of the 2d elastic wave equations in frequency-domain. We have, for $\mathbf{x} = (x, z) \in \Omega \subset \mathbb{R}^2$

$$\begin{cases} i\omega\rho(\mathbf{x})\mathbf{v}(\mathbf{x}) &= \mathbf{div}\left(\underline{\underline{\sigma}}(\mathbf{x})\right) & \text{in } \Omega, \\ i\omega\underline{\underline{\sigma}}(\mathbf{x}) &= \underline{\underline{C}}(\mathbf{x})\,\underline{\underline{\epsilon}}(\mathbf{v}(\mathbf{x})) + \underline{\underline{f}}(\mathbf{x}) & \text{in } \Omega, \end{cases} \tag{1}$$

where i is the imaginary unit, ω the angular frequency; $\rho(\mathbf{x})$ defines the mass density and $\underline{\underline{f}}(\mathbf{x})$ the source term which is generally associated to volume forces. The vector $\mathbf{v}(\mathbf{x}) = (v_x(\mathbf{x}), v_z(\mathbf{x}))^T$ is the velocity field and $\underline{\underline{\epsilon}}$ the strain tensor, where $\epsilon_{jk} = \dfrac{1}{2}\left(\dfrac{\partial v_j}{\partial k} + \dfrac{\partial v_k}{\partial j}\right), \quad j,k = x,z$. The tensor $\underline{\underline{\sigma}}$ is the stress tensor. In the general case, $\sigma_{jk} = \displaystyle\sum_{l=x}^{z}\sum_{m=x}^{z} C_{jklm}\epsilon_{lm}$ and in the particular isotropic case, $\sigma_{jk} = \lambda\delta_{jk}tr(\underline{\underline{\epsilon}}) + 2\mu\epsilon_{jk}, \quad j,k = x,z$, with λ and μ Lame's coefficients. The tensor $\underline{\underline{C}}$ is a fourth order symmetric tensor containing the elastic coefficients. Using Voigt's notation

$$jk \to \alpha \text{ or } lm \to \beta = 11 \to 1, \quad 22 \to 2, \quad 12 \to 3.$$

we reduce it to a 3×3 matrix. In the general anisotropic case we have

$$\underline{\underline{C}}(\mathbf{x}) = \begin{pmatrix} C_{11}(\mathbf{x}) & C_{12}(\mathbf{x}) & C_{13}(\mathbf{x}) \\ C_{12}(\mathbf{x}) & C_{22}(\mathbf{x}) & C_{23}(\mathbf{x}) \\ C_{13}(\mathbf{x}) & C_{23}(\mathbf{x}) & C_{33}(\mathbf{x}) \end{pmatrix},$$

while in the isotropic case

$$\underline{\underline{C}}(\mathbf{x}) = \begin{pmatrix} \lambda(\mathbf{x}) + 2\mu(\mathbf{x}) & \lambda(\mathbf{x}) & 0 \\ \lambda(\mathbf{x}) & \lambda(\mathbf{x}) + 2\mu(\mathbf{x}) & 0 \\ 0 & 0 & \mu(\mathbf{x}) \end{pmatrix}.$$

Thereafter, we do not write space dependencies for physical parameters ρ, λ and μ, tensors $\underline{\underline{C}}, \underline{\underline{\sigma}}$ and $\underline{\underline{\epsilon}}$ and $\mathbf{v}$. We also assume that physical parameters (ρ, λ and μ for the isotropic case, and ρ and the C_{ij} coefficients in the general case) are piece-wise constant. We can develop the equations of system (1). We have for $(x, z) \in \Omega \subset \mathbb{R}^2$

$$\left\{\begin{array}{l} i\omega v_x = \dfrac{1}{\rho}\left(\dfrac{\partial \sigma_{xx}}{\partial x} + \dfrac{\partial \sigma_{xz}}{\partial z}\right), \\ i\omega v_z = \dfrac{1}{\rho}\left(\dfrac{\partial \sigma_{xz}}{\partial x} + \dfrac{\partial \sigma_{zz}}{\partial z}\right), \\ i\omega \sigma_{xx} = C_{11}\dfrac{\partial v_x}{\partial x} + C_{12}\dfrac{\partial v_z}{\partial z} + C_{13}\left(\dfrac{\partial v_x}{\partial z} + \dfrac{\partial v_z}{\partial x}\right) + f_{xx}, \\ i\omega \sigma_{zz} = C_{12}\dfrac{\partial v_x}{\partial x} + C_{22}\dfrac{\partial v_z}{\partial z} + C_{23}\left(\dfrac{\partial v_x}{\partial z} + \dfrac{\partial v_z}{\partial x}\right) + f_{zz}, \\ i\omega \sigma_{xz} = C_{13}\dfrac{\partial v_x}{\partial x} + C_{23}\dfrac{\partial v_z}{\partial z} + C_{33}\left(\dfrac{\partial v_x}{\partial z} + \dfrac{\partial v_z}{\partial x}\right) + f_{xz}, \end{array}\right. \tag{2}$$

The boundary conditions are given by

$$\underline{\underline{\sigma}}\mathbf{n} = 0 \quad \text{on } \Gamma_l, \tag{3}$$

$$\underline{\underline{\sigma}}\mathbf{n} + \mathbf{P}\mathbf{A}(\theta')\mathbf{P}^T\mathbf{v} = 0 \quad \text{on } \Gamma_a, \tag{4}$$

where $\Gamma_l \cup \Gamma_a = \partial\Omega$ and $\Gamma_l \cap \Gamma_a = \emptyset$, $\mathbf{n}$ the outward unitary norm vector and $\mathbf{t}$ the associated tangential vector, which is such that $(\mathbf{n}, \mathbf{t})$ is a direct orthonormal basis of $\mathbb{R}^2$. Relation (3) defines a free surface condition whereas (4) represents an absorbing boundary condition (ABC) in the anisotropic case. The matrices $\mathbf{P}$ and $\mathbf{A}$ are defined by

$$\mathbf{P} = \begin{pmatrix} n_x & -n_z \\ n_z & n_x \end{pmatrix}$$

and

$$\mathbf{A}(\theta) = \begin{pmatrix} a_{11}(\theta) & a_{12}(\theta) \\ a_{21}(\theta) & a_{22}(\theta) \end{pmatrix} \text{ with } \left\{\begin{array}{rcl} a_{11}(\theta) &=& -\rho v_p f(\theta)\left(\kappa\cos^2\theta + \sin^2\theta\right), \\ a_{12}(\theta) &=& -\rho v_p f(\theta)\left(-(\kappa-1)\cos\theta\sin\theta\right), \\ a_{21}(\theta) &=& -\rho v_p g(\theta)\left(-(\kappa\cos^2\theta + \sin^2\theta)\right), \\ a_{22}(\theta) &=& -\rho v_p g(\theta)\left((\kappa-1)\cos\theta\sin\theta\right) - \rho v_s, \\ f(\theta) &=& \dfrac{\kappa\cos^2\theta + \sin^2\theta}{\sqrt{\kappa^2\cos^2\theta + \sin^2\theta}}, \\ g(\theta) &=& \dfrac{(\kappa-1)\cos\theta\sin\theta}{\sqrt{\kappa^2\cos^2\theta + \sin^2\theta}}. \end{array}\right.$$

The ABC is the one proposed in (Barucq *et al.* 2014) and is restricted to tilted transverse isotropic (TTI) media. The parameter v_p is the P-wave velocity, v_s the S-wave velocity, θ is the tilted angle of

the wave in the TTI medium and $\kappa = \sqrt{1-2\varepsilon}$, with ε being one of Thomsen's constants defining the TTI nature of the medium and expressed by $\varepsilon = \dfrac{C_{11}-C_{13}}{2C_{33}}$. We refer to (Thomsen 1986) for more informations about Thomsen's parameters and weak elastic anisotropy. The angle θ' is defined such as

$$\begin{cases} \cos\theta' = -n_z \sin\theta + n_x \cos\theta, \\ \\ \sin\theta' = \sqrt{1-\cos^2\theta'}. \end{cases}$$

In the isotropic case, $\theta = 0$ and thus the expression of matrix $\mathbf{A}(\theta)$ reduces to

$$\mathbf{A}(\theta) = \begin{pmatrix} -\rho v_p & 0 \\ 0 & -\rho v_s \end{pmatrix}$$

and thus, the condition (4) reads as

$$\underline{\underline{\sigma}}\mathbf{n} - \rho v_p(\mathbf{v}\cdot\mathbf{n})\mathbf{n} - \rho v_s(\mathbf{v}\cdot\mathbf{t})\mathbf{t} = 0 \text{ on } \Gamma_a. \tag{5}$$

It might seems odd to consider the first order formulation when ones wants to reduce the size of the linear system. Indeed, working directly with the second order formulation allows to eliminate directly the stress unknowns and to consider two (respectively three) unknowns instead of five (respectively nine) in 2D (respectively in 3D). The principle of HDG consists in introducing an auxiliary unknown of dimension two (respectively three) that replaces the stresses and the displacement in the solution of the linear system. If the gain with respect to classical methods for first order formulation is obvious, it might not be clear to the reader that there is also a gain with respect to classical methods for second order formulations. We should now precise that the auxiliary unknown is defined only on the edges (respectively the faces) of the mesh, while the unknown of classical methods for second order formulation are volumic. Hence, assuming that a 2D mesh with N vertices is composed of $\dfrac{N}{2}$ elements and $\dfrac{N}{3}$ edges, a p order HDG method will lead to $\dfrac{2(p-1)N}{3}$ degrees of freedom, while a classical DG method for second order formulation would require $\dfrac{3(p+1)(p+2)N}{4}$ degrees of freedom, a classical CG method for second order formulation $3\dfrac{N+(p-1)N+(p-1)(p-2)N}{2} = 3N\dfrac{p+(p-1)(p-2)}{2}$. Hence, for p large enough, the HDG method is the one which requires the less number of degrees of freedom. We will provide numerical comparison in the numerical results section that illustrate this point.

Moreover, as far as we know, the HDG methodology has never been adapted to second order wave problems (except of course by transforming the second order into a first order system before applying HDG, as it is done in (Nguyen, Peraire, & Cockburn 2011b)). Even if it were possible to design a HDG method, the size of the global linear system would remain the same as first order HDG and the

only gain would lie in the construction and in the final resolution steps, which are two embarassingly parallel tasks.

3 HDG METHOD

In this section, we first introduce the notations and the functional spaces required to derive the variational formulation, then we present the continuous HDG formulation and its discretization.

3.1 Notations

We define the dot product between two vectors $\mathbf{v}$ and $\mathbf{u}$ as $\mathbf{v} \cdot \mathbf{u}$, and between two tensors $\underline{\underline{\xi}}$ and $\underline{\underline{\zeta}}$ as $\underline{\underline{\xi}} : \underline{\underline{\zeta}}$. We also define the tensorial product between two vectors $\mathbf{v}$ and $\mathbf{u}$ as $\mathbf{v} \otimes \mathbf{u}$.

We consider a triangulation $\mathcal{T}_h$ of Ω. Then

- $\mathcal{F}(K)$ denotes the set of the faces of an element K of $\mathcal{T}_h$,
- F is a face of K,
- $\mathcal{F}_b$ denotes the set of boundary faces F_b, i.e. $F_b = \partial K \cap \Gamma$, where $\Gamma = \partial\Omega$,
- $\mathcal{F}_a$ denotes the set of absorbing boundary faces F_a, i.e. $F_a = \partial K \cap \Gamma_a$,
- $\mathcal{F}_l$ denotes the set of free surface faces F_l, i.e. $F_l = \partial K \cap \Gamma_l$,
- $\mathcal{F}_i$ denotes the set of interior faces F_i, i.e. $F_i = \partial K \cap \partial K'$ where K and K' are neighbors,
- $\mathcal{F}_h$ denotes the set of all the faces of the mesh, i.e. $\mathcal{F}_h = \mathcal{F}_i \cup \mathcal{F}_b$,
- $\mathbf{n}$ denotes the outward unit normal vector to K and $\mathbf{t}$ the associated tangential vector, which is such that $(\mathbf{n}, \mathbf{t})$ is a direct orthonormal basis of $\mathbb{R}^2$.

Since we use discontinuous functions, we have to compute their jump and mean at the interface between two elements. For an interior face $F = \partial K^+ \cap \partial K^- \in \mathcal{F}_i$ we define the jump $[\![\cdot]\!]$ and the mean $\{\cdot\}$ of a vector $\mathbf{v}$ as

$$[\![\mathbf{v}]\!] = \mathbf{v}^+ - \mathbf{v}^- \text{ and } \{\mathbf{v}\} = \frac{\mathbf{v}^+ + \mathbf{v}^-}{2}.$$

For a boundary face $F = \partial K^+ \cap \Gamma \in \mathcal{F}_b$, the jump and the mean reduce to

$$[\![\mathbf{v}]\!] = \mathbf{v}^+ \text{ and } \{\mathbf{v}\} = \frac{\mathbf{v}}{2}.$$

The jump and the mean of a tensor $\underline{\underline{\sigma}}$ are defined for an interior face $F \in \mathcal{F}_i$ as

$$[\![\underline{\underline{\sigma}}]\!] = \underline{\underline{\sigma}}^+\mathbf{n}^+ + \underline{\underline{\sigma}}^-\mathbf{n}^-, \text{ and } \{\underline{\underline{\sigma}}\} = \frac{\underline{\underline{\sigma}}^+\mathbf{n}^+ + \underline{\underline{\sigma}}^-\mathbf{n}^+}{2}$$

and for a boundary face $F \in \mathcal{F}_b$ as

$$[\![\underline{\underline{\sigma}}]\!] = \underline{\underline{\sigma}}^+\mathbf{n}^+ \text{ and } \{\underline{\underline{\sigma}}\} = \frac{\underline{\underline{\sigma}}^+\mathbf{n}^+}{2}.$$

We denote by $P_p(D)$ the set of polynomials of degree at most p on the domain D. For each element $K \in \mathcal{T}_h$, we define $\mathbf{V}^p(K)$ as the space $(P_p(K))^2$ and $\mathbf{\Sigma}^p(K)$ as the space $(P_p(K))^3$. We introduce the discontinuous finite element spaces

$$\mathbf{V}_h^p = \{\mathbf{v} \in \left(L^2(\Omega)\right)^2 \text{ such that } \quad \mathbf{v}|_K \in \mathbf{V}^p(K), \forall K \in \mathcal{T}_h\},$$
$$\mathbf{\Sigma}_h^p = \{\underline{\underline{\sigma}} \in \left(L^2(\Omega)\right)^3 \text{ such that } \quad \underline{\underline{\sigma}}|_K \in \mathbf{\Sigma}^p(K), \forall K \in \mathcal{T}_h\},$$

where $L^2(\Omega)$ is the space of square integrable functions on the domain Ω. These two functional spaces are composed of functions that are continuous inside each element of the mesh, but discontinuous at the interfaces between two elements.

Finally, we define for each face $F \in \mathcal{F}_h$ the space $\mathbf{M}^p(F)$ as the space $(P_p(F))^2$ and we introduce the traced finite element space

$$\mathbf{M}_h = \{\boldsymbol{\eta} \in \left(L^2(\mathcal{F}_h)\right)^2 \text{ such that } \quad \boldsymbol{\eta}|_F \in \mathbf{M}^p(F), \forall F \in \mathcal{F}_h\}.$$

This last functional space is composed of functions defined on the edges of the meshes. These functions are continuous on the edge but discontinuous at the intersection of two edges.

3.2 Formulation

We consider equations (1) on an element K of $\mathcal{T}_h$. We assume that the physical parameters ρ and $\underline{\underline{C}}$ are piece-wise constant, i.e. on a given element K, they are equal to ρ_K and $\underline{\underline{C}}_K$. The *classical* discontinuous Galerkin method seeks an approximate solution $(\mathbf{v}_h, \underline{\underline{\sigma}}_h)$ in the space $\mathbf{V}_h^p \times \mathbf{\Sigma}_h^p$ satisfying for all K in $\mathcal{T}_h$ and for all $(\mathbf{w}, \underline{\underline{\xi}})$ in $\mathbf{V}_h^p \times \mathbf{\Sigma}_h^p$

$$\left\{ \begin{array}{rcl} \displaystyle\int_K i\omega\rho_K \mathbf{v}_h \cdot \mathbf{w} - \int_K \mathbf{div}\left(\underline{\underline{\sigma}}_h\right) \cdot \mathbf{w} & = & 0, \\ \displaystyle\int_K i\omega \underline{\underline{\sigma}}_h : \underline{\underline{\xi}} - \int_K \left(\underline{\underline{C}}_K \underline{\underline{\epsilon}}(\mathbf{v}_h)\right) : \underline{\underline{\xi}} & = & \displaystyle\int_K \underline{\underline{f}} : \underline{\underline{\xi}}. \end{array} \right. \tag{6}$$

Integrating by parts, we obtain

$$\left\{ \begin{array}{rcl} \displaystyle\int_K i\omega\rho_K \mathbf{v}_h \cdot \mathbf{w} + \int_K \underline{\underline{\sigma}}_h : \underline{\underline{\nabla}}\mathbf{w} - \int_{\partial K} \left(\widehat{\underline{\underline{\sigma}}}_h \mathbf{n}\right) \cdot \mathbf{w} & = & 0, \\ \displaystyle\int_K i\omega \underline{\underline{\sigma}}_h : \underline{\underline{\xi}} + \int_K \mathbf{v}_h \cdot \left(\mathbf{div}\left(\underline{\underline{C}}_K \underline{\underline{\xi}}\right)\right) - \int_{\partial K} \widehat{\mathbf{v}}_h \cdot \left(\underline{\underline{C}}_K \underline{\underline{\xi}} \mathbf{n}\right) & = & \displaystyle\int_K \underline{\underline{f}} : \underline{\underline{\xi}}. \end{array} \right. \tag{7}$$

We now introduce numerical traces $\widehat{\underline{\underline{\sigma}}}_h$ and $\widehat{\mathbf{v}}_h$ which are respectively the approximations of $\underline{\underline{\sigma}}_h$ and $\mathbf{v}_h$ on ∂K. The principle of the HDG formulation is to express $(\widehat{\mathbf{v}}_h, \widehat{\underline{\underline{\sigma}}}_h)$ in terms of a hybrid unknown $\boldsymbol{\lambda}_h$ only. This unknown $\boldsymbol{\lambda}_h \in \mathbf{M}_h$ is a Lagrange multiplier and is here introduced to replace the numerical trace $\widehat{\mathbf{v}}_h$. This is written as

$$\widehat{\mathbf{v}}_h = \boldsymbol{\lambda}_h, \quad \forall F \in \mathcal{F}_h, \quad \boldsymbol{\lambda}_h \in \mathbf{M}_h. \tag{8}$$

Then, we define the numerical trace $\widehat{\underline{\underline{\sigma}}}_h$ in terms of the other unknowns through the relation

$$\widehat{\underline{\underline{\sigma}}}_h = \underline{\underline{\sigma}}_h - \left(\underline{\underline{S}}\left(\mathbf{v}_h - \boldsymbol{\lambda}_h\right)\right) \otimes \mathbf{n} \qquad \text{on } \partial K. \tag{9}$$

The tensor $\underline{\underline{S}}$ is a local stabilization matrix which has an important effect on both the accuracy and stability of the HDG scheme. Note that we have deduced the numerical trace (9) from the one adopted in (Nguyen, Peraire, & Cockburn 2011a) where the authors consider the displacement gradient-velocity-pressure formulation of the elastodynamic equations, and define

$$\mu\widehat{\mathbf{H}}_h + \widehat{p}_h\mathbf{I} = \mu\mathbf{H}_h + p_h\mathbf{I} - \left(\underline{\underline{S}}\left(\mathbf{v}_h - \widehat{\mathbf{v}}_h\right)\right) \otimes \mathbf{n}, \tag{10}$$

where $\mathbf{H} = \underline{\underline{\nabla}}\mathbf{u}$ is the displacement gradient tensor and $p = (\mu + \lambda)(\mathbf{div}\,(\mathbf{u}))$ is the hydrostatic pressure. Since

$$\mathbf{div}\left(\mu\mathbf{H}_h^n + p_h^n\mathbf{I}\right) = \mathbf{div}\left(\underline{\underline{\sigma}}_h\right), \tag{11}$$

and assuming that

$$\mathbf{div}\left(\mu\widehat{\mathbf{H}}_h^n + \widehat{p}_h^n\mathbf{I}\right) = \mathbf{div}\left(\widehat{\underline{\underline{\sigma}}}_h\right), \tag{12}$$

and then replacing $\left(\mu\widehat{\mathbf{H}}_h^n + \mathbf{div}\left(\widehat{p}_h^n\mathbf{I}\right)\right)$ in this equation by its definition given by (10), we find that

$$\mathbf{div}\left(\widehat{\underline{\underline{\sigma}}}_h\right) = \mathbf{div}\left(\underline{\underline{\sigma}}_h - \left(\underline{\underline{S}}\left(\mathbf{v}_h - \widehat{\mathbf{v}}_h\right)\right) \otimes \mathbf{n}\right), \tag{13}$$

yielding the definition (9). Moreover, in (Nguyen, Peraire, & Cockburn 2011a), it is proved from the energy identity that the tensor $\underline{\underline{S}}$ should have the form $\tau\underline{\underline{I}}$ where $\tau > 0$ is a local stabilization parameter and $\underline{\underline{I}}$ the identity matrix. Thanks to the dimensional analysis, we deduce that the unit of the penalization parameter τ is kg.s^{-1}.m^{-2}. We assess the impact of this parameter on the accuracy of the solution in section 4.2.

System (7) is closed by imposing the weak continuity of the normal component of $\widehat{\underline{\underline{\sigma}}}_h$, so that the problem can be rewritten in the following way: find $(\mathbf{v}_h, \underline{\underline{\sigma}}_h, \boldsymbol{\lambda}_h) \in \mathbf{V}_h^p \times \boldsymbol{\Sigma}_h^p \times \mathbf{M}_h$ such that $\forall K \in \mathcal{T}_h$, $\forall F \in \mathcal{F}_h$ and $\forall(\mathbf{w}, \underline{\underline{\xi}}, \boldsymbol{\eta}) \in \mathbf{V}^p(K) \times \boldsymbol{\Sigma}^p(K) \times \mathbf{M}^p(F)$

$$\left\{\begin{array}{lcl} \displaystyle\int_K i\omega\rho_K\mathbf{v}_h \cdot \mathbf{w} + \int_K \underline{\underline{\sigma}}_h : \underline{\underline{\nabla}}\mathbf{w} - \int_{\partial K}\left(\widehat{\underline{\underline{\sigma}}}_h\mathbf{n}\right)\cdot\mathbf{w} & = & 0, \\ \displaystyle\int_K i\omega\underline{\underline{\sigma}}_h : \underline{\underline{\xi}} + \int_K \mathbf{v}_h \cdot \left(\mathbf{div}\left(\underline{\underline{C}}_K\underline{\underline{\xi}}\right)\right) - \int_{\partial K}\boldsymbol{\lambda}_h \cdot \left(\underline{\underline{C}}_K\underline{\underline{\xi}}\mathbf{n}\right) & = & \displaystyle\int_K \underline{\underline{f}} : \underline{\underline{\xi}}, \\ \displaystyle\int_F [\![\widehat{\underline{\underline{\sigma}}}_h]\!]\cdot\boldsymbol{\eta} & = & 0. \end{array}\right. \tag{14}$$

We remark that the continuity of the normal component of $\widehat{\underline{\underline{\sigma}}}_h$ is weakly imposed by the last equation of (14) which is called the *conservativity condition*. According to (9), we note that on ∂K

$$\widehat{\underline{\underline{\sigma}}}_h\mathbf{n} = \underline{\underline{\sigma}}_h\mathbf{n} - \underline{\underline{S}}\left(\mathbf{v}_h - \widehat{\mathbf{v}}_h\right). \tag{15}$$

It is clear that for a face $F = \partial K^+ \cap \partial K^-$

$$\int_F [\![\widehat{\underline{\underline{\sigma}}}_h]\!] \cdot \boldsymbol{\eta} = \int_F \left(\underline{\underline{\sigma}}_h^{K^+} \mathbf{n}^{K^+} - \underline{\underline{S}}^{K^+} \left(\mathbf{v}_h^{K^+} - \widehat{\mathbf{v}}_h \right) \right) \cdot \boldsymbol{\eta}$$

$$+ \int_F \left(\underline{\underline{\sigma}}_h^{K^-} \mathbf{n}^{K^-} - \underline{\underline{S}}^{K^-} \left(\mathbf{v}_h^{K^-} - \widehat{\mathbf{v}}_h \right) \right) \cdot \boldsymbol{\eta},$$

thus

$$\int_F [\![\widehat{\underline{\underline{\sigma}}}_h]\!] \cdot \boldsymbol{\eta} = \int_F [\![\underline{\underline{\sigma}}_h]\!] \cdot \boldsymbol{\eta} - \int_F 2\underline{\underline{S}} \left(\{\mathbf{v}_h\} - \widehat{\mathbf{v}}_h \right) \cdot \boldsymbol{\eta}.$$

For a face $F \in \mathcal{F}_l$,

$$\int_F [\![\widehat{\underline{\underline{\sigma}}}_h]\!] \cdot \boldsymbol{\eta} = \int_F \left(\widehat{\underline{\underline{\sigma}}}_h \mathbf{n} \right) \cdot \boldsymbol{\eta} = \int_F \mathbf{g}_l \cdot \boldsymbol{\eta},$$

where $\mathbf{g}_l$ is the value that we impose on the Dirichlet boundary, and here we assume $\mathbf{g}_l = 0$. Replacing $\widehat{\underline{\underline{\sigma}}}_h \mathbf{n}$ by the expression (15), we obtain the following expression for the Dirichlet condition

$$\int_F [\![\underline{\underline{\sigma}}_h]\!] \cdot \boldsymbol{\eta} - \int_F 2\underline{\underline{S}} \left(\{\mathbf{v}_h\} - \widehat{\mathbf{v}}_h \right) \cdot \boldsymbol{\eta} = 0.$$

For a face $F \in \mathcal{F}_a$,

$$\int_F [\![\widehat{\underline{\underline{\sigma}}}_h]\!] \cdot \boldsymbol{\eta} = \int_F \left(\widehat{\underline{\underline{\sigma}}}_h \mathbf{n} \right) \cdot \boldsymbol{\eta} = \int_F \mathbf{g}_a \cdot \boldsymbol{\eta},$$

where $\mathbf{g}_a$ is the value that we impose on the absorbing boundary, and here we assume $\mathbf{g}_a = -\mathbf{PA}(\theta)\mathbf{P}^T \widehat{\mathbf{v}}_h$. Replacing $\widehat{\underline{\underline{\sigma}}}_h \mathbf{n}$ by the expression (15), we obtain the following expression for an absorbing boundary

$$\int_F [\![\underline{\underline{\sigma}}_h]\!] \cdot \boldsymbol{\eta} - \int_F 2\underline{\underline{S}} \left(\{\mathbf{v}_h\} - \boldsymbol{\lambda}_h \right) \cdot \boldsymbol{\eta} + \int_F \left(\mathbf{PA}(\theta)\mathbf{P}^T \boldsymbol{\lambda}_h \right) \cdot \boldsymbol{\eta} = 0.$$

Now, in order to obtain a global HDG formulation, we rewrite system (14) as

$$\left\{ \begin{array}{lcl} \displaystyle\int_K i\omega\rho_K \mathbf{v}_h \cdot \mathbf{w} - \int_K \left(\mathbf{div} \underline{\underline{\sigma}}_h \right) \cdot \mathbf{w} + \int_{\partial K} \underline{\underline{S}} \left(\mathbf{v}_h - \boldsymbol{\lambda}_h \right) \cdot \mathbf{w} & = & 0, \\ \displaystyle\int_K i\omega \underline{\underline{\sigma}}_h : \underline{\underline{\xi}} + \int_K \mathbf{v}_h \cdot \left(\mathbf{div} \left(\underline{\underline{C}}_K \underline{\underline{\xi}} \right) \right) - \int_{\partial K} \boldsymbol{\lambda}_h \cdot \left(\underline{\underline{C}}_K \underline{\underline{\xi}} \mathbf{n} \right) & = & \displaystyle\int_K \underline{\underline{f}} : \underline{\underline{\xi}}, \\ \displaystyle\int_F [\![\underline{\underline{\sigma}}_h]\!] \cdot \boldsymbol{\eta} - \int_F 2\underline{\underline{S}} \left(\{\mathbf{v}_h\} - \boldsymbol{\lambda}_h \right) \cdot \boldsymbol{\eta} + \int_{F \in \mathcal{F}_a} \left(\mathbf{PA}(\theta)\mathbf{P}^T \boldsymbol{\lambda}_h \right) \cdot \boldsymbol{\eta} & = & 0. \end{array} \right. \tag{16}$$

If $\boldsymbol{\lambda}_h$ is known, then the restriction of the solution to the element K, $\left(\mathbf{v}_h^K, \underline{\underline{\sigma}}_h^K \right) = \left(\mathbf{v}_{h|K}, \underline{\underline{\sigma}}_{h|K} \right)$, can be computed by solving the local HDG problem : find $\left(\mathbf{v}_h^K, \underline{\underline{\sigma}}_h^K \right) \in (\mathbf{V}^p(K) \times \boldsymbol{\Sigma}^p(K))$ such as $\forall \left(\mathbf{w}, \underline{\underline{\xi}} \right) \in (\mathbf{V}^p(K) \times \boldsymbol{\Sigma}^p(K))$

$$\left\{ \begin{array}{lcl} \displaystyle\int_K i\omega\rho_K \mathbf{v}_h^K \cdot \mathbf{w} - \int_K \left(\mathbf{div} \left(\underline{\underline{\sigma}}_h^K \right) \right) \cdot \mathbf{w} + \int_{\partial K} \underline{\underline{S}} \left(\mathbf{v}_h^K - \boldsymbol{\lambda}_h \right) \cdot \mathbf{w} & = & 0, \\ \displaystyle\int_K i\omega \underline{\underline{\sigma}}_h^K : \underline{\underline{\xi}} + \int_K \mathbf{v}_h^K \cdot \left(\mathbf{div} \left(\underline{\underline{C}}_K \underline{\underline{\xi}} \right) \right) - \int_{\partial K} \boldsymbol{\lambda}_h \cdot \left(\underline{\underline{C}}_K \underline{\underline{\xi}} \mathbf{n} \right) & = & \displaystyle\int_K \underline{\underline{f}}^K : \underline{\underline{\xi}}. \end{array} \right. \tag{17}$$

Because of the additional unknown $\boldsymbol{\lambda}_h$, it is *a priori* more difficult to analyze the properties of system (16) than the ones of classical first order DG schemes. However, we show in appendix A

that (16) can be rewritten actually as a first order DG scheme, involving only the original unknown $\mathbf{v}_h$ and $\underline{\underline{\sigma}}_h$. Hence, it is possible to study the HDG scheme similarly to classical DG schemes.

In appendix B, we describe the discretization of the variational formulation and we discuss the implementation aspects. The discretization is done in two steps: first, we discretize the local HDG equations for the 2D elastodynamics (17) (appendix B1) and then we use the condition transmission i.e. the last equation of system (16) to obtain the global linear system (appendix B2) . We show in particular that the global linear system characterizing the HDG scheme only involves the degrees of freedom of the Lagrange multiplier $\boldsymbol{\lambda}_h$ (appendix B3). Finally, we demonstrate the symmetry of the global linear HDG system (appendix B4).

4 NUMERICAL RESULTS

In this section, we provide 2d numerical results in order to assess the performances of the proposed HDG method in terms of accuracy and efficiency. This HDG method has been implemented in a Fortran 90 software. We use the sparse direct solver MUMPS (see (Amestoy, Duff, & L'Excellent 2000) for more details) for the resolution of the linear system for the hybrid unknown. Numerical experiments are performed on a hardware system equipped with quad-core Nehalem Intel® Xeon® X5550/2,66 GHz CPUs and 24 GB (DDR3 1333 MHz) of RAM. All the computer codes that we have used in the following numerical study were not implemented with the same level of optimization. Therefore, in order to avoid discrepancies due to the parallelization of the codes, all the results presented below were computed in sequential mode.

In section 4.2, we study the numerical convergence of the HDG method by considering the propagation of a plane wave in a homogeneous isotropic medium, where we can compute an analytical solution. We also compare the HDG results with those obtained with an upwind flux-based DG method. Then, we focus on more geophysical examples. We first consider an anisotropic problem, for which we compare the HDG solution to the one obtained with a more classical DG scheme, the IPDG formulation. Finally, we compare the HDG method with classical continuous finite elements on the Marmousi benchmark.

4.1 General remarks

We detail in appendix C the algorithms of the various methods we use. It is worth noting that the construction step of all codes has been implemented differently and maybe not optimally. However, the solution of the linear solver is performed by the same linear solver (MUMPS) for all the codes. Hence, even if we give the numerical costs of the construction of the matrix for the sake of completeness, the

most significant results are the ones related to the linear solver. It is also important to mention that the construction step and the additional reconstruction step for HDG are embarrassingly parallel, so that the bottleneck for computation lies in the linear solver. Since one code does not allow to take advantage of the symmetry of the matrix, we have decided not to use this option in the other codes in order to provide fair comparisons, except for the last experiment on the Marmousi case where we test both symmetric and non-symmetric versions of HDG.

4.2 Numerical convergence study

For the study of the numerical properties of the HDG method, we consider the simple test problem of the propagation of a plane wave in a homogeneous medium. The computational domain Ω is a 10 km $\times$ 10 km square. The physical properties of the medium are the density $\rho = 1$ kg.m^{-3} and the Lamé's parameters λ and μ that are set to 8 MPa and 4 MPa respectively. These values imply a velocity v_p of P-waves equal to 4 000 m.s^{-1} and a velocity v_s of S-waves equal to 2 000 m.s^{-1}. On the boundaries we impose an absorbing condition with a plane wave incident field $\mathbf{W}$

$$\mathbf{W} = \begin{pmatrix} V_{x0} \\ V_{z0} \\ \sigma_{xx0} \\ \sigma_{zz0} \\ \sigma_{xz0} \end{pmatrix} e^{i(k_x \cos\theta x + k_z \sin\theta z)},$$

where $k = \sqrt{k_x^2 + k_z^2}$ is the wavenumber, θ is the incidence angle and with

$$\begin{cases} V_{z0} = \dfrac{k_x k_z \left(\lambda + \mu\right)}{\rho\omega^2 - k_x^2\mu - k_z^2(\lambda + 2\mu)} V_{x0}, \\ \sigma_{xx0} = \dfrac{-1}{\omega}\left(k_x \left(\lambda + 2\mu\right) V_{x0} + \lambda k_z V_{z0}\right), \\ \sigma_{zz0} = \dfrac{-1}{\omega}\left(\lambda k_x V_{x0} + \left(\lambda + 2\mu\right) k_z V_{z0}\right), \\ \sigma_{xz0} = \dfrac{-\mu}{\omega}\left(k_z V_{x0} + k_x V_{z0}\right). \end{cases}$$

If we consider a P-wave for the simulation of the propagation of a plane wave, $k = \dfrac{\omega}{v_p}$, and thus $k_x = \dfrac{\omega}{v_p}\cos\theta$ and $k_z = \dfrac{\omega}{v_p}\sin\theta$. For a S-wave, $k = \dfrac{\omega}{v_s}$, and thus $k_x = \dfrac{\omega}{v_s}\cos\theta$ and $k_z = \dfrac{\omega}{v_s}\sin\theta$. Here, $\omega = 2\pi f$ denotes the angular frequency and f is the frequency. In the simulations, we choose $\theta = 0$ and $f = 2$ Hz, so that $\omega = 4\pi \simeq 12.56$ rad.s^{-1}. We discretize the computational domain Ω into three unstructured meshes with respectively 3 100, 10 300 and 45 000 elements. The characteristics of these meshes are given in Tab. 1. Figure 1 shows the numerical convergence of the HDG method for τ=1 kg.s^{-1}.m^{-2}. As with classical finite element methods or with an upwind flux-based DG (UDG)

Table 1. Plane wave propagation in a homogeneous medium. Characteristics of the three meshes.

Mesh	# Elements	# Vertices	h_{min}	h_{max}	$\frac{h_{max}}{h_{min}}$
M1	3 100	1 620	193.6 m	625.0 m	3.2
M2	10 300	5 200	107.5 m	312.5 m	2.9
M3	45 000	22 500	45.4 m	156.2 m	3.5

method, we observe a convergence of order $p+1$ when the interpolation order is p, i.e with optimal rate, on the whole solution, and particularly on the $\underline{\underline{\sigma}}$ components (see fig. 3). We have performed a similar study for different values of τ going from 10^{-4} to 10^{4}. In all cases, we obtain the same $p+1$ convergence order. However, the accuracy of the HDG solution depends on the value of the stabilization matrix $\mathbf{S}$. In our formulation, the stabilization matrix $\mathbf{S}$ is equal to $\tau\mathbf{I}$, where $\mathbf{I}$ is the identity matrix and τ the stabilization parameter. In order to assess the influence of the parameter τ on the accuracy of the computed solution, we thus study the variation of the relative error as a function of the value of the parameter τ. For several values of the interpolation degree p, we compute the numerical solution of the propagation of the plane wave on the second mesh (composed of 10 300 elements) while the parameter τ is varied from 10^{-4} to 10^{4}. In Figs. 4a to 4d, the relative error of the UDG solution (thick line) is considered as the reference for the comparison with the relative error of the HDG solution. We remark that, at least for this test case, when the value of the parameter τ is of the order of ρv_p (which is coherent with the dimensional analysis), we obtain the same relative error than with the UDG scheme. Moreover, we have increased the value of the parameter τ up to

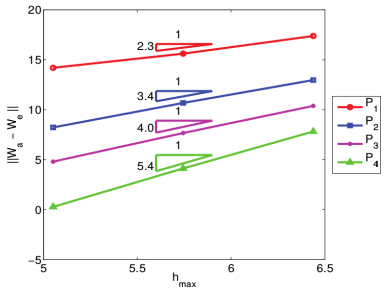

Figure 1. Plane wave propagation in a homogeneous medium. Convergence order of the HDG method for plane wave propagation in a homogeneous medium.

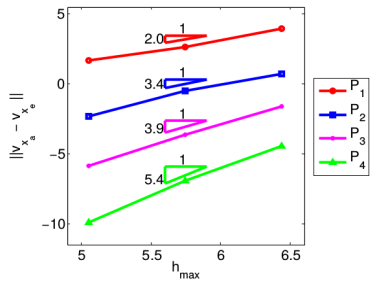

Figure 2. Plane wave propagation in a homogeneous medium. Convergence order of the HDG method on the v_x component for plane wave propagation in a homogeneous medium.

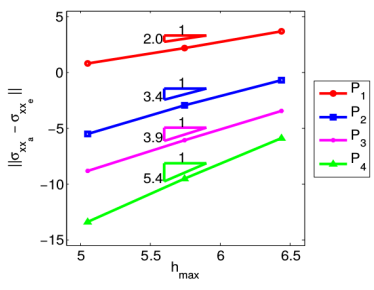

Figure 3. Plane wave propagation in a homogeneous medium. Convergence order of the HDG method on the σ_{xx} component for plane wave propagation in a homogeneous medium.

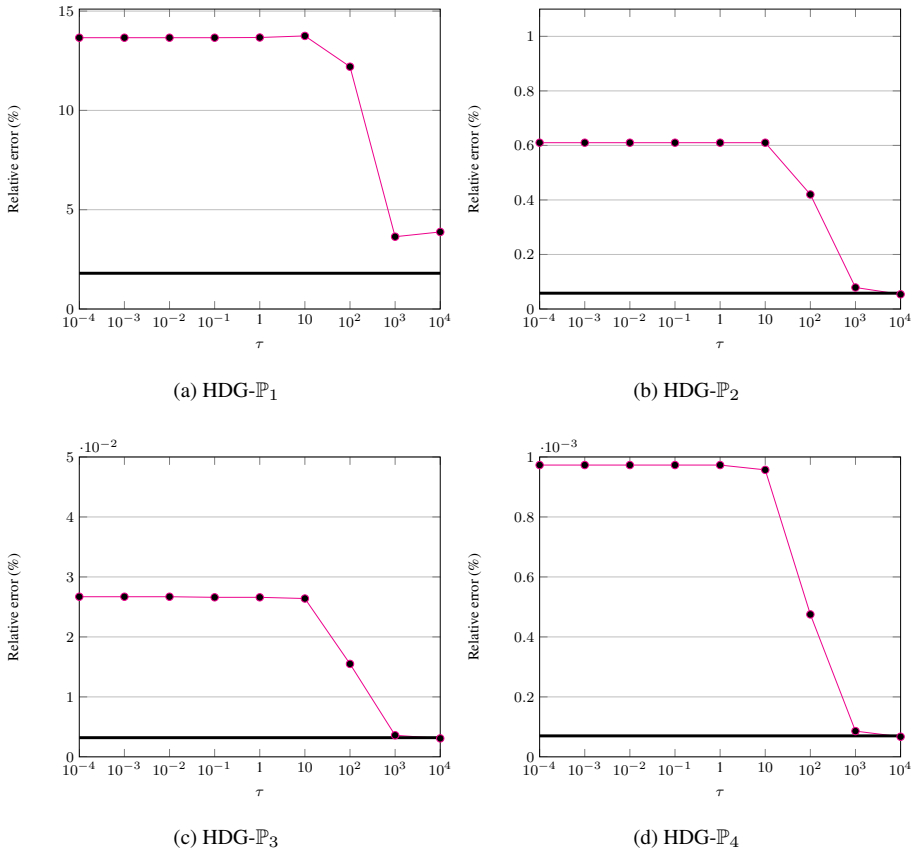

(a) HDG-$\mathbb{P}_1$ (b) HDG-$\mathbb{P}_2$

(c) HDG-$\mathbb{P}_3$ (d) HDG-$\mathbb{P}_4$

Figure 4. Plane wave propagation in a homogeneous medium. Influence of the parameter τ on the relative error using the same mesh and the same physical parameters.

the value $\lambda + 2\mu (\sim 10^6)$ and remarked that the relative error remains constant. In Figs. 5a to 5d, we plot the variation of the relative error as a function of the discretization step (i.e. mesh) when we set $\tau = \rho v_p$. Except for the HDG-$\mathbb{P}_1$ scheme, the behavior of the relative error is the same as the behavior of the relative error of the UDG scheme. We note that in (Terrana, Vilotte, & Guillot 2015), the expression of the stabilization matrix $\mathbf{S}$ is derived in terms of the physical parameters of the media by using a Riemann solver. In Tabs. 2 and 3, we present the characteristics of the mesh for a given error level with different interpolation degrees. We also specify the number of degrees of freedom per wavelength $n_w = \frac{ndof}{\lambda_w} = \frac{ndof}{\frac{v_p}{f}}$. The results presented so far have been obtained for a P-plane wave. We have also tested the HDG method for a S-plane wave, i.e for $k = \frac{\omega}{v_s}$. Setting $\tau^K = \rho v_s^K$ as the local value of the stabilization parameter, we also obtain an optimal convergence rate for the HDG method.

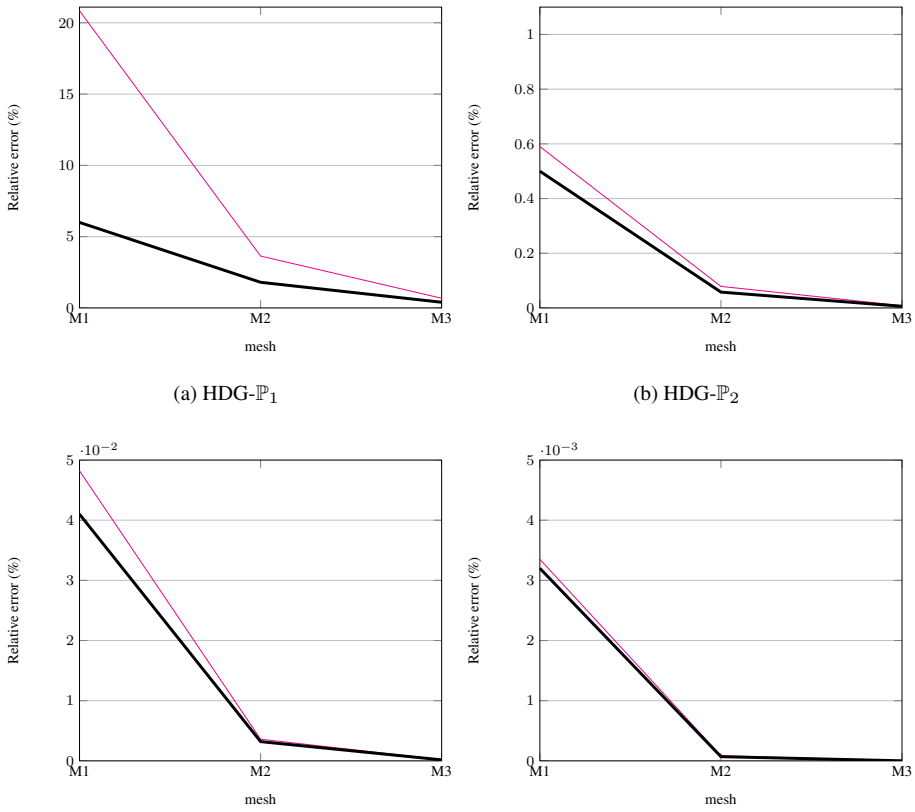

(a) HDG-$\mathbb{P}_1$ (b) HDG-$\mathbb{P}_2$

(c) HDG-$\mathbb{P}_3$ (d) HDG-$\mathbb{P}_4$

Figure 5. Plane wave propagation in a homogeneous medium. Variation of the relative error as a function of the mesh for the UDG scheme (**–**) and for the HDG scheme (–) when $\tau = \rho v_p$.

4.3 Anisotropic problem

We apply here the proposed HDG method to a problem involving anisotropic media. We consider the domain shown on Fig. 6. The physical characteristics of the six media of this model are summarized in Tab. 4. The computational domain is reduced to a 3 km $\times$ 3 km square. On the upper boundary, we impose the free surface condition (3) while on the other boundaries, we apply the absorbing condition

p	# elements	# vertices	h_{max} (m)	h_{min} (m)	n_w
1	22 300	11 300	184.6	70.1	67
2	1 600	800	670.8	279.2	7
3	580	320	1 250.0	454.9	4
4	230	130	2500.0	742.3	2

Table 2. Plane wave propagation in a homogeneous medium. Characteristics of the meshes in order to reach an accuracy level of 1% on V_x for $\tau = \rho v_p$ (p is the interpolation degree).

p	# elements	# vertices	h_{max} (m)	h_{min} (m)	n_w
1	78 000	39 000	99.1	24.6	233
2	6 500	3 340	323.6	136.3	28
3	1 600	840	641.6	275.4	10
4	780	420	1 250.0	394.7	6

Table 3. Plane wave propagation in a homogeneous medium. Characteristics of the meshes in order to reach an accuracy level of 0.1% on V_x for $\tau = \rho v_p$ (p is the interpolation degree).

(4). The computational domain is discretized into three unstructured meshes with respectively 600, 3 000 and 28 000 elements. Their characteristics are given in Tab. 5. The frequency f is set to 12 Hz. The acoustic medium (the layer of water) is approximated with a pseudo-acoustic medium, i.e., we considered an elastic medium with $v_s = 0$ m.s^{-1}. The HDG solution, shown in Fig. 8a was computed with $\tau^K = v_p^K$ in each cell. For this test case, as we do not have access to an analytical solution, we compare the HDG results with the one obtained with the IPDG method (see Fig. 8b). Both methods deliver similar solutions as we can see in Figs. 8a and 8b. It is also interesting to look at the computational performances of the two methods (Tab. 7). The HDG formulation is more competitive in terms of memory and computational time than the IPDG method: it requires at least 3 times less memory and 3 times less computational time. We recall that in the HDG memory occupancy data, we have included the memory required by the linear system solver and the memory that we need to store the matrices for the computation of the degrees of freedom of the element-wise fields. The HDG resolution time includes the linear system solver time and the time to obtain the element-wise fields. Finally we also compare in Tab. 6 the computational performances of the HDG method for isotropic and anisotropic problem settings. We clearly see that taking into account the anisotropy does not increase the computational cost. This is due to the fact that, in the HDG formulation, the anisotropic property affects only two local matrices and more specifically affects only the value of some coefficients which do not vanish in the isotropic case neither.

4.4 Comparison with classical finite elements on the Marmousi problem

To conclude this series of numerical results, we compare the HDG method to a classical finite elements method, the continuous Galerkin method (CG) and the IPDG method on a classical geophysical test case, the Marmousi problem (see Fig. 9). On a same mesh composed of 139 000 elements and using the same interpolation degree, we compare the numerical solutions (see Fig. 10), the total number of degrees of freedom of each method and the number of non-zero terms in each global matrix (see Tab.

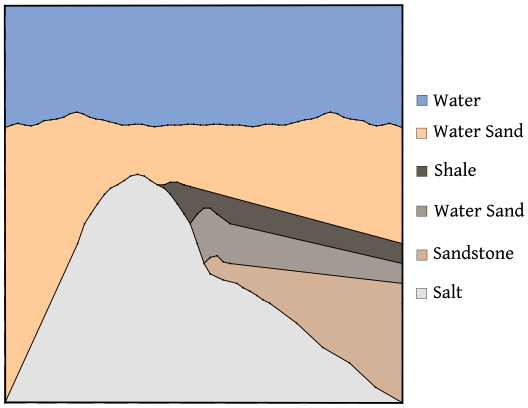

Figure 6. Anisotropic problem. Configuration of the computational domain Ω.

8). Then, in Tab. 9, we compare the memory required by the solver and the total memory used for the simulation. Finally, in Tab. 10 we compare the computational time for the factorization of the global matrix. In these tables, we use the symmetric option of the solver to factorize the CG and IPDG global matrix; for the HDG global matrix, we have decided to use both options: the symmetric one and the unsymmetric one in order to emphasize the advantage to use a symmetric numerical method. In terms of accuracy, if we compare the numerical solutions (see Fig. 10), we obtain similar numerical solutions with the three methods. Regarding the total memory, the classical CG method appears to be the better solution. But as we explain in section C4, in our algorithm we choose to store the matrices that we need for the reconstruction of the initial solution, thus we can reduce the HDG total memory for a simulation by reconstructing these matrices. As they are local and independent, their computation can be performed in parallel. For computational costs, with this example, we remark that if we only focus on the memory used by the solver, the symmetric HDG method is as competitive as the classical CG

	Water	Water Sand 1	Shale	Water Sand 2	Sandstone	Salt
v_p	1 500	1 409	4 359	1 609	4 633	5 334
v_s	0	480	3 048	780	3 231	3 353
ρ	1 000	2 030	2 810	2 030	2 710	2 710
ϵ	0	0.22	0.172	022	-0.026	0.369
δ	0.0	0.018	0.0	0.018	-0.033	0.579
θ	0.0	0.0	10.0	15.0	25.0	20.0

Table 4. Anisotropic problem. Characteristics of the anisotropic media. Units: v_p and v_s in m.s^{-1}; ρ in kg.m^{-3}; θ in degree.

Mesh	# elements	# vertices	h_{min} (m)	h_{max} (m)	$\frac{h_{max}}{h_{min}}$
M1	600	330	30	512	17.07
M2	3 000	1 500	30	187.5	6.25
M3	28 000	14 180	13.6	64.9	4.77

Table 5. Anisotropic problem. Characteristics of the three meshes.

method, while the IPDG method requires more memory. More precisely, the symmetric HDG method requires more memory than CG up to order 5, and then becomes less expensive. It should be noted that we only consider here conform meshes; we expect the symmetric HDG method to be even less expensive when using hp-adaptivity.

5 CONCLUSION

We have proposed in this paper a new discontinuous Galerkin type method for the numerical solution of the frequency-domain elastodynamic equations in 2d. This hybridizable discontinuous Galerkin formulation allows to drastically reduce the number of globally coupled degrees of freedom resulting in lower execution time and memory occupation as compared to a classical discontinuous Galerkin formulation, while preserving all the advantages of the latter with regards to high order accuracy and flexibility in handling unstructured meshes. Our future works will address the extension of the formulation to the 3d case including the design of a parallel solution strategy for the system of linear equations for the hybrid variable. We will also work on the elasto-acoustic coupling in order to improve the simulation when we consider several media and to reduce potential pollution effects.

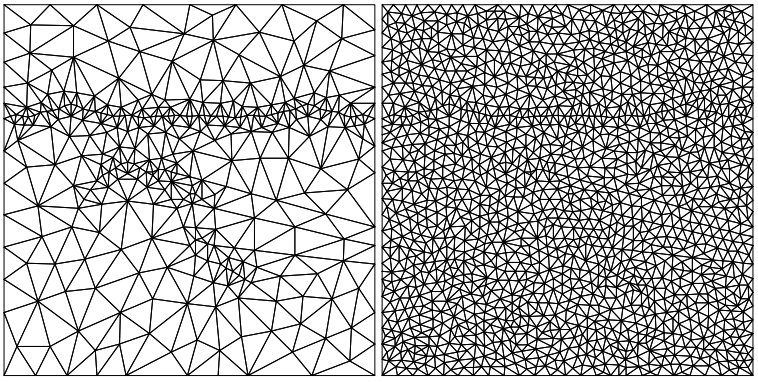

(a) Mesh M1 with 600 elements (b) Mesh M2 with 3 000 elements

Figure 7. Anisotropic problem. Discretization of the domain Ω.

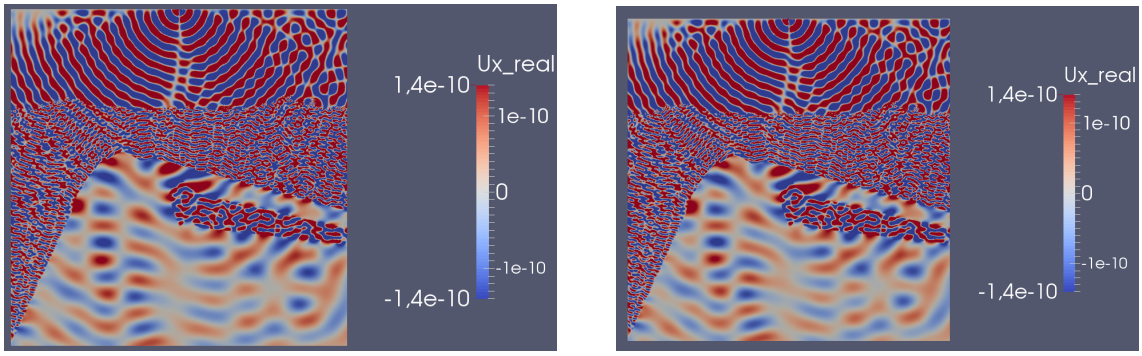

(a) HDG-$\mathbb{P}_4$ (b) IPDG-$\mathbb{P}_4$

Figure 8. Anisotropic problem. Left: HDG-$\mathbb{P}_4$ numerical solution for $\tau^K = v_p^K$. Right: IPDG-$\mathbb{P}_4$ numerical solution, mesh M3

ACKNOWLEDGMENTS

We would like to acknowledge Prof. Jean Virieux for the useful discussions and suggestions.

This work has been supported by the Inria-TOTAL strategic action DIP (http://dip.inria.fr), the Marie Curie RISE action GEAGAM (http://sites.google.com/site/geagamnetwork) and the EU-Brazil project HPC4E (hpc4e.eu).

Graphics presented in this paper were obtained using the visualization application Paraview, see (Ahrens, Geveci, & Law 2005) and (Ayachit & Utkarsh 2015) for more details.

Experiments presented in this paper were carried out using the PLAFRIM experimental testbed, being developed under the Inria PlaFRIM development action with support from Bordeaux INP, LABRI and IMB and other entities: Conseil Rgional d'Aquitaine, Universit de Bordeaux and CNRS (and ANR in accordance to the programme dinvestissements dAvenir (see https://www.plafrim.fr/).

Mesh	Memory (MB)		Construction time (s)		Solution time (s)	
	Iso.	Aniso.	Iso.	Aniso.	Iso.	Aniso.
M1	50	50	0.4	0.3	1.0	1.0
M2	222	222	1.9	1.3	5.5	4.1
M3	2 485	2 485	12.3	12.4	49.7	44.2

Table 6. Anisotropic problem: comparison between isotropic (iso.) and anisotropic (aniso.) HDG-$\mathbb{P}_3$ performances.

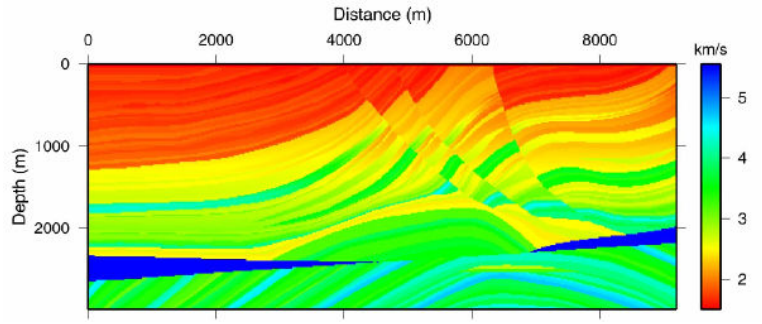

Figure 9. Marmousi test case. Configuration of the computational domain Ω and v_p-velocity model.

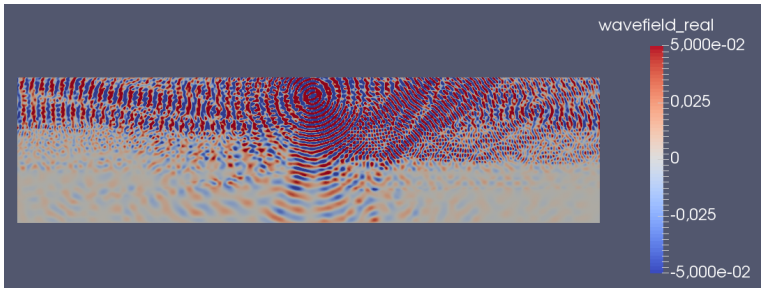

(a) CG-$\mathbb{P}_5$

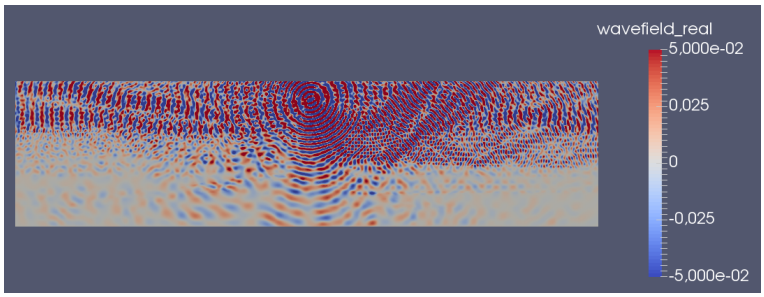

(b) IPDG-$\mathbb{P}_5$

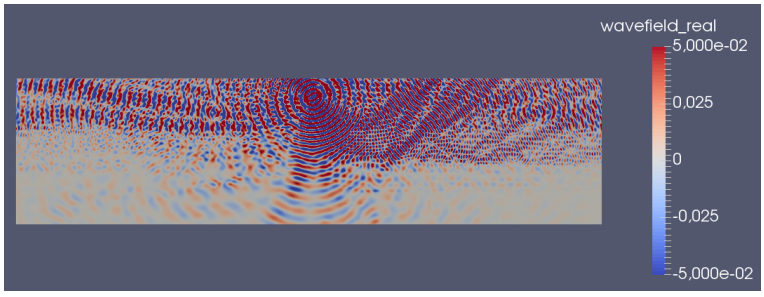

(c) HDG-$\mathbb{P}_5$

Figure 10. Marmousi test case. 10a CG-$\mathbb{P}_5$ numerical solution. 10b IPDG-$\mathbb{P}_5$ numerical solution. 10c HDG-$\mathbb{P}_5$ numerical solution with $\tau = v_p$.

Mesh	Memory (MB)		Construction time (s)		Solution time (s)	
	HDG	IPDG	HDG	IPDG	HDG	IPDG
M1	75	217	0.7	2.3	1.7	4.6
M2	353	1 274	3.3	10.0	8.1	25.0
M3	4 041	17 328	35.3	105.0	88.6	368.0

Table 7. Anisotropic problem: comparison between HDG-$\mathbb{P}_4$ and IPDG-$\mathbb{P}_4$ performances.

Interpolation degree	# dof			# non-zero			
	CG	HDG	IPDG	CG	HDG	HDG sym.	IPDG
3	1.3e6	1.7e6	2.8e6	2.2e7	6.7e7	3.4e7	9.9e7
4	2.2e6	2.1e6	4.2e6	5.3e7	1.0e8	5.3e7	2.1e8
5	3.5e6	2.5e6	5.8e6	1.1e8	1.5e8	7.6e7	4.1e8
6	5.0e6	2.9e6	7.8e6	2.0e8	2.0e8	1.0e8	7.1e8

Table 8. Marmousi test case. HDG vs. CG vs. IPDG: comparison of the number of degrees of freedom, and of the number of non-zero terms.

Interpolation degree	Solver memory (GB)				Grid and other data memory (GB)				Local matrices memory (GB)			
	CG	HDG	HDG sym.	IPDG	CG	HDG	HDG sym.	IPDG	CG	HDG	HDG sym.	IPDG
3	2.6	6.8	4.6	14.0	0.8	0.8	0.8	0.8	0.0	0.5	0.5	0.0
4	5.3	10.1	6.6	24.7	0.8	0.8	0.8	0.8	0.0	1.5	1.5	0.0
5	8.6	14.2	9.2	38.3	0.8	0.9	0.9	0.9	0.0	3.1	3.1	0.0
6	13.4	19.1	12.5	63.0	0.8	0.9	0.9	0.9	0.0	5.2	5.2	0.0

Table 9. Marmousi test case. HDG vs. CG vs. IPDG: comparison of the memory needed by the solver, and of the total memory used for the simulation.

Interpolation degree	Factorization time (s)			
	CG	HDG	HDG sym.	IPDG
3	9	13	10	42
4	15	21	15	58
5	22	27	20	143
6	38	37	25	-

Table 10. Marmousi test case. HDG vs. CG vs. IPDG: comparison of the factorization time.

REFERENCES

Ahrens, J., Geveci, B. & Law, C. 2005. ParaView: An End-User Tool for Large Data Visualization. Number ISBN-13: 978-0123875822. Visualization Handbook, elsevier edition, 2005.

Ainsworth, M., Monk, P. & Muniz, W., 2006. Dispersive and dissipative properties of discontinuous Galerkin finite element methods for the second-order wave equation, *J. Sci. Comp.*. **27**, 5-40.

Arnold, D. N., Brezzi, F., Cockburn, B., & Marini, D. (2000). Discontinuous Galerkin methods for elliptic problems. Lecture notes in computational science and engineering, 11, 89-102.

Amestoy, P.R., Duff, I.S. & L'Excellent, J.-Y., 2000. Multifrontal parallel distributed symmetric and unsymmetric solvers, *Comput. Meth. App. Mech. Engng.*. **184**, 501-520.

Ayachit & Utkarsh 2015. The ParaView Guide: A Parallel Visualization Application. Kitware, ISBN 978-1930934306 edition, 2015.

Baldassari, C., Barucq, H., Calandra, H., Denel, B. & Diaz, J., 2012. Performance analysis of a high-order discontinuous Galerkin method. Application to the reverse time migration, *Comm. Comput. Phys.*. **11(2)**, 660–673.

Barucq, H., Boillot, L., Calandra, H. & Diaz, J., 2014. Absorbing Boundary Conditions for 2D Tilted Transverse Isotropic Media *ESAIM: Proceedings*. **45**, pp.400-409

Barucq, H., Djellouli, R., & Estecahandy, E., 2014. Efficient DG-like formulation equipped with curved boundary edges for solving elasto-acoustic scattering problems. *Intern. J. Numer. Meth. Engng.*, **98(10)**, 747-780.

Bonnasse-Gahot, M. (2015). High order discontinuous Galerkin methods for time-harmonic elastodynamics, PhD. thesis, *Université Nice Sophia Antipolis*).

Brossier, R., Etienne, V., Operto, S. & Virieux, J., 2010. Frequency-domain numerical modelling of visco-acoustic waves with finite-difference and finite-element discontinuous Galerkin methods, *INTECH Open Access Publisher*.

Cockburn, B., Gopalakrishnan, J. & Lazarov, R., 2009. Unified hybridization of discontinuous Galerkin, mixed and continuous Galerkin methods for second order elliptic problems, *SIAM J. Numer. Anal.*. **47**, 1319-1365.

Cockburn, B., Karniadakis, G. E., & Shu, C. W. (2000). The development of discontinuous Galerkin methods. In Discontinuous Galerkin Methods (pp. 3-50). Springer, Berlin, Heidelberg.

Delcourte, S., Fezoui, L. & Glinsky-Olivier, N., 2009. A high-order discontinuous Galerkin method for the seismic wave propagation. ESAIM: Proc.. **27**, 70–89.

Di Pietro, D. A., & Ern, A. (2011). Mathematical aspects of discontinuous Galerkin methods (Vol. 69). Springer Science & Business Media.

Dumbser, M. & Käser, M., 2006. An arbitrary high-order discontinuous Galerkin method for elastic waves on unstructured meshes - II. The three-dimensional isotropic case. *Geophys. J. Intern.*. **167(1)**, 319–336.

Dumbser, M., Käser, M. & Toro, E.F., 2007. An arbitrary high-order discontinuous Galerkin method for elastic waves on unstructured meshes - V. Local time stepping and p-adaptivity. *Geophys. J. Intern.*. **171(2)**, 695–717.

El Bouajaji, M. & Lanteri, S., 2013. High order discontinuous Galerkin method for the solution of 2D time-

harmonic Maxwell's equations. *Appl. Math. Comp.*, **219(13)**, 7241-7251.

Etienne, V., Chaljub, E., Virieux, J. & Glinsky-Olivier, N., 2010. An hp-adaptive discontinuous Galerkin finite-element method for 3-D elastic wave modelling. *Geophys. J. Intern.*, **183(2)**, 941–962.

Ern, A. & Guermond, J.-L., 2006. Discontinuous Galerkin methods for Friedrich's systems. I. General theory. *SIAM J. Numer. Anal.*, **44(2)**, 753–778.

Ern, A. & Guermond, J.-L., 2006. Discontinuous Galerkin methods for Friedrich's systems. I. Second-order elliptic PDE's. *SIAM J. Numer. Anal.*, **44(6)**, 2363–2388.

Fezoui, L., Lanteri, S., Lohrengel, S. & Piperno, S., 2005. Convergence and stability of a discontinuous Galerkin time-domain method for the 3D heterogeneous Maxwell equations on unstructured meshes. *ESAIM: Math. Model. and Numer. Anal.*. **39(6)**, 1149–1176.

Giorgiani, G., Modesto, D., Fernández-Méndez, S., & Huerta, A. (2013). High-order continuous and discontinuous Galerkin methods for wave problems. International Journal for numerical methods in Fluids, 73(10), 883-903.

Giorgiani, G., Modesto, D., Fernández-Méndez, S., & Huerta, A. (2013). Hybridizable discontinuous Galerkin p–adaptivity for wave propagation problems. International Journal for Numerical Methods in Fluids, 72(12), 1244-1262.

Grote, M.J., Schneebeli, A. & and Schötzau, D., 2006. Discontinuous Galerkin finite element method for the wave equation. *SIAM J. Numer. Anal.*. **44(6)**, 2408–2431.

Grote, M.J., Schneebeli, A. & Schötzau, D., 2008. Interior penalty discontinuous Galerkin method for Maxwell's equations: optimal L^2-norm error estimates. *IMA J. Numer. Anal.*. **28(3)**, 440–468.

Grote, M.J. & Schötzau, D., 2009. Optimal error estimates for the fully discrete interior penalty DG method for the wave equation. *J. Sci. Comp.*. **40**, 257–272.

Hesthaven, J. S., & Warburton, T. (2007). Nodal discontinuous Galerkin methods: algorithms, analysis, and applications. Springer Science & Business Media.

Käser, M. & and Dumbser, M., 2006. An arbitrary high-order discontinuous Galerkin method for elastic waves on unstructured meshes - I. The two-dimensional isotropic case with external source terms. *Geophys. J. Intern.*, **166(2)**, 855–877.

Kirby, R.M., Sherwin, S.J., & Cockburn, B., 2012. To CG or to HDG: a comparative study, *J. Sci. Comp.*. **51**, 183-212.

Lanteri, S. Li, L. & Perrussel, R., 2013. Numerical investigation of a high order hybridizable discontinuous Galerkin method for 2d time-harmonic Maxwell's equations, *COMPEL*. **32(3)**, 1112-1138.

Marfurt, K., 1984. Accuracy of finite difference and finite element modeling of the scalar and elastic wave equation. *Geophys.*. **49**, 533–549.

Min, J.D., Shin, C., Pratt, R.G. & Yoo, H.S., 2003. Weighted-averaging finite-element method for 2d elastic wave equations in the frequency domain. *Bul. Seism. Soc. Amer.*. **93**, 904–921.

Nguyen, N.C., Peraire, J. & Cockburn, B., 2009. An implicit high-order hybridizable discontinuous Galerkin method for linear convection-diffusion equations, *J. Comput. Phys.*. **228(9)**, 3232-3254.

Nguyen, N.C., Peraire, J. & Cockburn, B., 2009. An implicit high-order hybridizable discontinuous Galerkin method for nonlinear convection-diffusion equations, *J. Comput. Phys.*. **228(23)**, 8841–8855.

Nguyen, N.C., Peraire, J. & Cockburn, B., 2011. High-order implicit hybridizable discontinuous Galerkin methods for acoustics and elastodynamics, *J. Comput. Phys.*. **230(10)**, 3695–3718.

Nguyen, N.C., Peraire, J. & Cockburn, B., 2011. Hybridizable discontinuous Galerkin methods for the time-harmonic Maxwell's equations, *J. Comput. Phys.*. **230(19)**, 7151–7175.

Nguyen, N.C. & Peraire, J., 2012. Hybridizable discontinuous Galerkin methods for partial differential equations in continuum mechanics, *J. Comput. Phys.*. **231(15)**, 5955–5988.

Piperno, S., Remaki, M. & Fezoui, L., 2002. A nondiffusive finite volume scheme for the three-dimensional Maxwell's equations on unstructured meshes. *SIAM J. Numer. Anal.*. **39(6)**, 2089–2108.

Reed, W. H., & Hill, T. R. (1973). Triangular mesh methods for the neutron transport equation (No. LA-UR–73-479; CONF-730414–2). Los Alamos Scientific Lab., N. Mex.(USA).

Rivière, B. (2008). Discontinuous Galerkin methods for solving elliptic and parabolic equations: theory and implementation. *SIAM*.

Tago, J., Cruz-Atienza, V.M., Virieux, J., Etienne, V. & Sánchez-Sesma, F.J., 2013. A 3D hp-adaptive discontinuous Galerkin method for modeling earthquake dynamics. *J. Geophys. Research: Solid Earth*. **117**, B09312.

Terrana, S., Vilotte, J.P. & Guillot, L. 2015. New high-order, semi-implicit Hybridized Discontinuous Galerkin - Spectral Element Method (HDG-SEM) for the simulation of complex wave propagation involving coupling between seismic, hydro-acoustic and infrasonic waves: numerical analysis and case studies. S23C-2760, American Geophysical Union Fall Meeting abstracts, San Francisco, 2015.

Thomsen, L., 1986. Weak elastic anisotropy. *Geophysics*. **51(10)**, 1954–1966.

Wilcox, L. C., Stadler, G., Burstedde, C., & Ghattas, O. (2010). A high-order discontinuous Galerkin method for wave propagation through coupled elastic–acoustic media. *J. Comput. Phys.*. 229(24), 9373–9396.

APPENDIX A: RELATIONSHIP BETWEEN HDG AND UPWIND FLUX-BASED DG

As we have three unknowns, i.e. $\mathbf{v}$, $\boldsymbol{\lambda}$ and $\underline{\underline{\sigma}}$, the properties of the previously introduced HDG scheme are more difficult to establish than the ones of classical DG methods. In this section, we elaborate on the relationship between the HDG scheme and the upwind flux-based nodal DG method in order to reduce at two variables. This show that the properties of HDG schemes can be studied similarly to the properties of classical DG schemes. We assume here that the tensor $\underline{\underline{S}}$ is invertible and that the source term vanishes. To simplify the presentation, we also assume that $\underline{\underline{S}}$ is uniquely defined on each face. The transmission condition reads as

$$\int_F 2\underline{\underline{S}}\boldsymbol{\lambda}_h^F \cdot \boldsymbol{\eta} \;=\; \int_F 2\underline{\underline{S}}\{\mathbf{v}_h\} \cdot \boldsymbol{\eta} - \int_F [\![\underline{\underline{\sigma}}_h]\!] \cdot \boldsymbol{\eta}.$$

Setting $\tilde{\boldsymbol{\eta}} = 2\underline{\underline{S}}^T\boldsymbol{\eta}$ we get that

$$\int_F \boldsymbol{\lambda}_h^F \cdot \tilde{\boldsymbol{\eta}} \;=\; \int_F \{\mathbf{v}_h\}\cdot\tilde{\boldsymbol{\eta}} - \int_F \frac{\underline{\underline{S}}^{-1}}{2}[\![\underline{\underline{\sigma}}_h]\!]\cdot\tilde{\boldsymbol{\eta}}, \quad \forall F\in\mathcal{F}_h \text{ and } \forall\tilde{\boldsymbol{\eta}}\in\mathbf{M}^p(F).$$

Thanks to this expression, and after some tedious calculations that we omit here, we are able to express $\int_{\partial K}\underline{\underline{S}}\left(\mathbf{v}_h^K-\boldsymbol{\lambda}_h\right)\cdot\mathbf{w}$ and $\int_{\partial K}\boldsymbol{\lambda}_h\cdot\left(\underline{\underline{C}}_K\underline{\xi}\mathbf{n}\right)$ in the two first equations of (16) in terms of $\mathbf{v}_h$ and σ_h yielding the problem : find $(\mathbf{v}_h,\underline{\underline{\sigma}}_h)\in\mathbf{V}_h^p\times\boldsymbol{\Sigma}_h^p$ such that $\forall K\in\mathcal{T}_h$ and $\forall(\mathbf{w},\underline{\xi})\in\mathbf{V}^p(K)\times\boldsymbol{\Sigma}^p(K)$

$$\begin{cases} \displaystyle\int_K i\omega\rho_K\mathbf{v}_h\cdot\mathbf{w}+\int_K\underline{\underline{\sigma}}_h:\underline{\underline{\nabla}}\mathbf{w}-\int_{\partial K}\{\underline{\underline{\sigma}}\}\cdot[\![\mathbf{w}]\!]-\int_{\partial K}\frac{\underline{\underline{S}}}{2}[\![\mathbf{v}]\!]\cdot[\![\mathbf{w}]\!]=0, \\ \displaystyle\int_K i\omega\underline{\underline{\sigma}}_h^K:\underline{\xi}+\int_K\mathbf{v}_h^K\cdot\left(\mathbf{div}\left(\underline{\underline{C}}_K\underline{\xi}\right)\right)-\int_{\partial K}\{\mathbf{v}\}\cdot[\![\underline{\underline{C}}_K\underline{\xi}\mathbf{n}]\!]+\int_{\partial K}\frac{\underline{\underline{S}}^{-1}}{2}[\![\underline{\underline{\sigma}}]\!]\cdot[\![\underline{\underline{C}}_K\underline{\xi}\mathbf{n}]\!]=0. \end{cases} \tag{A.1}$$

If the stabilization tensor is defined by $\underline{\underline{S}}=\tau\underline{\underline{I}}$, we get

$$\begin{cases} \displaystyle\int_K i\omega\rho_K\mathbf{v}_h\cdot\mathbf{w}+\int_K\underline{\underline{\sigma}}_h:\underline{\underline{\nabla}}\mathbf{w}-\int_{\partial K}\{\underline{\underline{\sigma}}\}\cdot[\![\mathbf{w}]\!]-\int_{\partial K}\frac{\tau}{2}[\![\mathbf{v}]\!]\cdot[\![\mathbf{w}]\!]=0, \\ \displaystyle\int_K i\omega\underline{\underline{\sigma}}_h^K:\underline{\xi}+\int_K\mathbf{v}_h^K\cdot\left(\mathbf{div}\left(\underline{\underline{C}}_K\underline{\xi}\right)\right)-\int_{\partial K}\{\mathbf{v}\}\cdot[\![\underline{\underline{C}}_K\underline{\xi}\mathbf{n}]\!]+\int_{\partial K}\frac{1}{2\tau}[\![\underline{\underline{\sigma}}]\!]\cdot[\![\underline{\underline{C}}_K\underline{\xi}\mathbf{n}]\!]=0. \end{cases} \tag{A.2}$$

System (A.2) shows that the HDG formulation can be interpreted locally as an upwind flux-based DG formulation. Similar upwind flux-based DG formulations can be found for acoustic in (Ainsworth, Monk, & Muniz 2006). The local HDG system has properties that are comparable to those of the upwind flux-based DG scheme and thus, it can be studied following the method proposed in (Ainsworth, Monk, & Muniz 2006). In particular, it can be shown that the stabilization parameter introduces numerical dissipation in the scheme. It is less straightforward to establish a link between other types of upwind fluxes, such as the one obtained for instance in (Wilcox *et al.* 2010) or in (El Bouajaji & Lanteri 2013) for electromagnetics. To do so, one has to integrate by part the two volumic terms

$$\int_K\underline{\underline{\sigma}}_h:\underline{\underline{\nabla}}\mathbf{w} \text{ and } \int_K\mathbf{v}_h^K\cdot\left(\mathbf{div}\left(\underline{\underline{C}}_K\underline{\xi}\right)\right)$$

in order to rewrite system (A.1) under a strong form. Note that we did not establish system (A.2) for the purpose of solving it, since this would require solving the global system which arises from it, but to reveal instead a coupling between the HDG formulation and an upwind flux-based DG formulation and to show that the HDG method can be studied locally as a classical DG scheme.

APPENDIX B: DISCRETIZATION AND IMPLEMENTATION ASPECTS

We detail here the discretization and the construction of the global linear system for the hybrid variable. For the sake of clarity, we first assume that the boundary conditions are periodic, so that we can consider that all the faces of the mesh are purely interior faces. Then, we include Dirichlet and absorb-

ing boundary conditions and we show how the boundary conditions modify the system. We focus on the discretization of the anisotropic case since the discretization of the isotropic case can be deduced from the anisotropic setting by replacing $C_{11} = C_{22} = \lambda + 2\mu,\ C_{12} = C_{21} = \lambda,\ C_{33} = \mu$ and $C_{13} = C_{23} = C_{31} = C_{32} = 0$.

B1 Discretization for periodic boundary conditions

We first consider periodic boundary conditions or, equivalently, that there is no boundary faces. For an element K, let $\left(\varphi_j^K\right)_{j=1,..,d_i^K}$ be the basis functions associated to element K with d_i^K the number of degrees of freedom. Taking the basis function φ_j^K as test function, we develop the local equations (17) for the anisotropic case and we write the local solution $(\mathbf{v}^K, \underline{\underline{\sigma}}^K)$ as a function of λ. Developing each equation of (17) separately, we have

$$\left\{\begin{array}{rcl} \displaystyle\int_K i\omega\rho_K v_x^K \varphi_j^K - \int_K \frac{\partial \sigma_{xx}^K}{\partial x}\varphi_j^K - \int_K \frac{\partial \sigma_{xz}^K}{\partial z}\varphi_j^K + \int_{\partial K} \tau^K v_x^K \varphi_j^K - \int_{\partial K} \tau^K \lambda_x \varphi_j^K &=& 0, \\ \displaystyle\int_K i\omega\rho_K v_z^K \varphi_j^K - \int_K \frac{\partial \sigma_{xz}^K}{\partial x}\varphi_j^K - \int_K \frac{\partial \sigma_{zz}^K}{\partial z}\varphi_j^K + \int_{\partial K} \tau^K v_z^K \varphi_j^K - \int_{\partial K} \tau^K \lambda_z \varphi_j^K &=& 0, \end{array}\right. \tag{B.1}$$

for the velocity and

$$\left\{\begin{array}{rcl} \displaystyle\int_K i\omega\sigma_{xx}^K\varphi_j^K &+& \displaystyle\int_K C_{11} v_x^K \frac{\partial \varphi_j^K}{\partial x} + \int_K C_{12} v_z^K \frac{\partial \varphi_j^K}{\partial z} + \int_K C_{13}\left(v_x^K \frac{\partial \varphi_j^K}{\partial z} + v_z^K \frac{\partial \varphi_j^K}{\partial x}\right) \\ &-& \displaystyle\int_{\partial K} C_{11}\lambda_x \varphi_j^K n_x - \int_{\partial K} C_{12}\lambda_z \varphi_j^K n_z - \int_{\partial K} C_{13}\left(\lambda_x \varphi_j^K n_z + \lambda_z \varphi_j^K n_x\right) = \int_K f_{xx}\varphi_j^K, \\ \displaystyle\int_K i\omega\sigma_{zz}^K\varphi_j^K &+& \displaystyle\int_K C_{12} v_x^K \frac{\partial \varphi_j^K}{\partial x} + \int_K C_{22} v_z^K \frac{\partial \varphi_j^K}{\partial z} + \int_K C_{23}\left(v_x^K \frac{\partial \varphi_j^K}{\partial z} + v_z^K \frac{\partial \varphi_j^K}{\partial x}\right) \\ &-& \displaystyle\int_{\partial K} C_{12}\lambda_x \varphi_j^K n_x - \int_{\partial K} C_{22}\lambda_z \varphi_j^K n_z - \int_{\partial K} C_{23}\left(\lambda_x \varphi_j^K n_z + \lambda_z \varphi_j^K n_x\right) = \int_K f_{zz}\varphi_j^K, \\ \displaystyle\int_K i\omega\sigma_{xz}^K\varphi_j^K &+& \displaystyle\int_K C_{13} v_x^K \frac{\partial \varphi_j^K}{\partial x} + \int_K C_{23} v_z^K \frac{\partial \varphi_j^K}{\partial z} + \int_K C_{33}\left(v_x^K \frac{\partial \varphi_j^K}{\partial z} + v_z^K \frac{\partial \varphi_j^K}{\partial x}\right) \\ &-& \displaystyle\int_{\partial K} C_{13}\lambda_x \varphi_j^K n_x - \int_{\partial K} C_{23}\lambda_z \varphi_j^K n_z - \int_{\partial K} C_{33}\left(\lambda_x \varphi_j^K n_z - \lambda_z \varphi_j^K n_x\right) = \int_K f_{xz}\varphi_j^K. \end{array}\right. \tag{B.2}$$

for the stress. We decompose the local solutions $(\mathbf{v}^K, \underline{\underline{\sigma}}^K)$ in the basis $\left(\varphi_j^K\right)$ as follows

$$\begin{aligned} v_l^K &= \sum_{j=1}^{d_i^K} \underline{v}_{l,j}^K \varphi_j^K, \qquad l = x, z, \\ \sigma_{kl}^K &= \sum_{j=1}^{d_i^K} \underline{\sigma}_{kl,j}^K \varphi_j^K, \qquad k, l = x, z. \end{aligned} \tag{B.3}$$

For a face F, λ is represented by

$$\lambda_l^F = \sum_{j=1}^{d_i^F} \underline{\lambda}_{l,j}^F \psi_j^F, \qquad l = x, z. \tag{B.4}$$

where $\left(\psi_j^F\right)_{j=1,..,d_i^F}$ are the basis functions of $P_p(F)$ and d_i^F the associated number of degrees of freedom. We denote by $\beta(K,l)$ the global index of the l-th face of the element K ($l = 1,2,3$). For example if the l-th face of K is the j-th face F_j then $\beta(K,l) = j$. Similarly, if F_l is the common face between K^e and K^f, we define $\alpha(l,+) = e$ and $\alpha(l,-) = f$. Then, after discretization, the local linear system resulting from (B.1)-(B.2) reads as

$$\left\{\begin{array}{rcl} i\omega\rho\mathbb{M}^K \underline{v}_x^K - \mathbb{D}_x^{K^T} \underline{\sigma}_{xx}^K - \mathbb{D}_z^{K^T} \underline{\sigma}_{xz}^K + \sum_{l=1}^3 \tau^{(K,l)} \mathbb{E}_l^K \underline{v}_x^K - \sum_{l=1}^3 \tau^{(K,l)} \mathbb{F}_l^K \underline{\lambda}_x^{\beta(K,l)} &=& 0, \\ i\omega\rho\mathbb{M}^K \underline{v}_z^K - \mathbb{D}_x^{K^T} \underline{\sigma}_{xz}^K - \mathbb{D}_z^{K^T} \underline{\sigma}_{zz}^K + \sum_{l=1}^3 \tau^{(K,l)} \mathbb{E}_l^K \underline{v}_z^K - \sum_{l=1}^3 \tau^{(K,l)} \mathbb{F}_l^K \underline{\lambda}_z^{\beta(K,l)} &=& 0, \end{array}\right. \tag{B.5}$$

for the velocity and

$$\left\{\begin{array}{rcl} i\omega\mathbb{M}^K \underline{\sigma}_{xx}^K &+& C_{11}^K \mathbb{D}_x^K \underline{v}_x^K + C_{12}^K \mathbb{D}_z^K \underline{v}_z^K + C_{13}^K \left(\mathbb{D}_x^K \underline{v}_z^K + \mathbb{D}_z^K \underline{v}_x^K\right) - \sum_{l=1}^3 C_{11}^K \underline{\lambda}_x^{\beta(K,l)} \mathbb{Q}_{xl}^K \\ &-& \sum_{l=1}^3 C_{12}^K \underline{\lambda}_z^{\beta(K,l)} \mathbb{Q}_{zl}^K - \sum_{l=1}^3 C_{13}^K \left(\underline{\lambda}_x^{\beta(K,l)} \mathbb{Q}_{zl}^K + \underline{\lambda}_z^{\beta(K,l)} \mathbb{Q}_{xl}^K\right) = \mathbb{M}^K \underline{f}_{xx}^K \\ i\omega\mathbb{M}^K \underline{\sigma}_{zz}^K &+& C_{12}^K \mathbb{D}_x^K \underline{v}_x^K + C_{22}^K \mathbb{D}_z^K \underline{v}_z^K + C_{23}^K \left(\mathbb{D}_x^K \underline{v}_z^K + \mathbb{D}_z^K \underline{v}_x^K\right) - \sum_{l=1}^3 C_{12}^K \underline{\lambda}_x^{\beta(K,l)} \mathbb{Q}_{xl}^K \\ &-& \sum_{l=1}^3 C_{22}^K \underline{\lambda}_z^{\beta(K,l)} \mathbb{Q}_{zl}^K - \sum_{l=1}^3 C_{23}^K \left(\underline{\lambda}_x^{\beta(K,l)} \mathbb{Q}_{zl}^K + \underline{\lambda}_z^{\beta(K,l)} \mathbb{Q}_{xl}^K\right) = \mathbb{M}^K \underline{f}_{zz}^K \\ i\omega\mathbb{M}^K \underline{\sigma}_{xz}^K &+& C_{13}^K \mathbb{D}_x^K \underline{v}_x^K + C_{23}^K \mathbb{D}_z^K \underline{v}_z^K + C_{33}^K \left(\mathbb{D}_x^K \underline{v}_z^K + \mathbb{D}_z^K \underline{v}_x^K\right) - \sum_{l=1}^3 C_{13}^K \underline{\lambda}_x^{\beta(K,l)} \mathbb{Q}_{xl}^K \\ &-& \sum_{l=1}^3 C_{23}^K \underline{\lambda}_z^{\beta(K,l)} \mathbb{Q}_{zl}^K - \sum_{l=1}^3 C_{33}^K \left(\underline{\lambda}_x^{\beta(K,l)} \mathbb{Q}_{zl}^K + \underline{\lambda}_z^{\beta(K,l)} \mathbb{Q}_{xl}^K\right) = \mathbb{M}^K \underline{f}_{xz}^K, \end{array}\right. \tag{B.6}$$

for the stress. The entries of the local matrices appearing in (B.5)-(B.6) are defined by

$$\begin{cases} \mathbb{M}_{ij}^K = \displaystyle\int_K \varphi_i^K \varphi_j^K \, d\mathbf{x}, \\ \mathbb{D}_{u,ij}^K = \displaystyle\int_K \varphi_i^K \partial_u \varphi_j^K \, d\mathbf{x}, \quad \text{with } u = x, z, \\ \mathbb{E}_{l,ij}^K = \displaystyle\int_{\partial K^l} \varphi_i^K \varphi_j^K \, ds, \\ \mathbb{F}_{l,ij}^K = \displaystyle\int_{\partial K^l} \psi_i^{\beta(K,l)} \varphi_j^K \, ds, \\ \mathbb{Q}_{ul,ij}^K = \displaystyle\int_{\partial K^l} n_u^K \psi_i^{\beta(K,l)} \varphi_j^K, \quad \text{with } u = x, z. \end{cases}$$

where ∂K^l denotes the face of index l of the element K. From (B.5)-(B.6), we gather the unknowns of the initial problem in a vector $\underline{W}^K$ such as $\underline{W}^K = \left(\underline{v}_x^K, \ \underline{v}_z^K, \ \underline{\sigma}_{xx}^K, \ \underline{\sigma}_{zz}^K, \ \underline{\sigma}_{xz}^K\right)^T$ and the hybrid unknowns in a vector $\underline{\Lambda}^K$ such as
$\underline{\Lambda}^K = \left(\underline{\lambda}_x^{\beta(K,1)}, \ \underline{\lambda}_x^{\beta(K,2)}, \ \underline{\lambda}_x^{\beta(K,3)}, \ \underline{\lambda}_z^{\beta(K,1)}, \ \underline{\lambda}_z^{\beta(K,2)}, \ \underline{\lambda}_z^{\beta(K,3)}\right)^T$. The local linear system on the element K can be written as

$$\mathbb{A}^K \underline{W}^K + \mathbb{C}^K \underline{\Lambda}^K = \mathbb{S}^K. \tag{B.7}$$

The matrices $\mathbb{A}^K$ and $\mathbb{C}^K$ are block matrices given by

$$\mathbb{A}^K = \begin{bmatrix} \mathbb{A}_{11}^K & \mathbb{A}_{12}^K \\ \mathbb{A}_{21}^K & \mathbb{A}_{22}^K \end{bmatrix},$$

$$\text{with } \mathbb{A}_{11}^K = \begin{bmatrix} i\omega\rho\mathbb{M}^K + \widetilde{\mathbb{E}^K} & 0 \\ 0 & i\omega\rho\mathbb{M}^K + \widetilde{\mathbb{E}^K} \end{bmatrix}, \quad \mathbb{A}_{12}^K = \begin{bmatrix} -\mathbb{D}_x^{K^T} & 0 & -\mathbb{D}_z^{K^T} \\ 0 & -\mathbb{D}_z^{K^T} & -\mathbb{D}_x^{K^T} \end{bmatrix},$$

$$\mathbb{A}_{21}^K = \begin{bmatrix} C_{11}^K \mathbb{D}_x^K + C_{13}^K \mathbb{D}_z^K & C_{12}^K \mathbb{D}_z^K + C_{13}^K \mathbb{D}_x^K \\ C_{12}^K \mathbb{D}_x^K + C_{23}^K \mathbb{D}_z^K & C_{22}^K \mathbb{D}_z^K + C_{23}^K \mathbb{D}_x^K \\ C_{13}^K \mathbb{D}_x^K + C_{33}^K \mathbb{D}_z^K & C_{23}^K \mathbb{D}_z^K + C_{33}^K \mathbb{D}_x^K \end{bmatrix}, \quad \mathbb{A}_{22}^K = \begin{bmatrix} i\omega\mathbb{M}^K & 0 & 0 \\ 0 & i\omega\mathbb{M}^K & 0 \\ 0 & 0 & i\omega\mathbb{M}^K \end{bmatrix}.$$

$$\text{where } \widetilde{\mathbb{E}^K} = \sum_{l=1}^{3} \tau^{(K,l)} \mathbb{E}_l^K,$$

$$\mathbb{C}^K = \begin{bmatrix} \mathbb{C}_{11}^K & \mathbb{C}_{12}^K \\ \mathbb{C}_{21}^K & \mathbb{C}_{22}^K \end{bmatrix}$$

with

$$\mathbb{C}_{11}^K = -\begin{bmatrix} \tau^{(K,1)}\mathbb{F}_1^K & \tau^{(K,2)}\mathbb{F}_2^K & \tau^{(K,3)}\mathbb{F}_3^K \\ \\ 0 & 0 & 0 \end{bmatrix}, \mathbb{C}_{12}^K = -\begin{bmatrix} 0 & 0 & 0 \\ \\ \tau^{(K,1)}\mathbb{F}_1^K & \tau^{(K,2)}\mathbb{F}_2^K & \tau^{(K,3)}\mathbb{F}_3^K \end{bmatrix},$$

$$\mathbb{C}_{21}^K = -\begin{bmatrix} C_{11}^K\mathbb{Q}_{x1}^K + C_{13}^K\mathbb{Q}_{z1}^K & C_{11}^K\mathbb{Q}_{x2}^K + C_{13}^K\mathbb{Q}_{z2}^K & C_{11}^K\mathbb{Q}_{x3}^K + C_{13}^K\mathbb{Q}_{z3}^K \\ C_{12}^K\mathbb{Q}_{x1}^K + C_{23}^K\mathbb{Q}_{z1}^K & C_{12}^K\mathbb{Q}_{x2}^K + C_{23}^K\mathbb{Q}_{z2}^K & C_{12}^K\mathbb{Q}_{x3}^K + C_{23}^K\mathbb{Q}_{z3}^K \\ C_{13}^K\mathbb{Q}_{x1}^K + C_{33}^K\mathbb{Q}_{z1}^K & C_{13}^K\mathbb{Q}_{x2}^K + C_{33}^K\mathbb{Q}_{z2}^K & C_{13}^K\mathbb{Q}_{x3}^K + C_{33}^K\mathbb{Q}_{z3}^K \end{bmatrix},$$

and $$\mathbb{C}_{22}^K = -\begin{bmatrix} C_{12}^K\mathbb{Q}_{z1}^K + C_{13}^K\mathbb{Q}_{x1}^K & C_{12}^K\mathbb{Q}_{z2}^K + C_{13}^K\mathbb{Q}_{x2}^K & C_{12}^K\mathbb{Q}_{z3}^K + C_{13}^K\mathbb{Q}_{x3}^K \\ C_{22}^K\mathbb{Q}_{z1}^K + C_{23}^K\mathbb{Q}_{x1}^K & C_{22}^K\mathbb{Q}_{z2}^K + C_{23}^K\mathbb{Q}_{x2}^K & C_{22}^K\mathbb{Q}_{z3}^K + C_{23}^K\mathbb{Q}_{x3}^K \\ C_{23}^K\mathbb{Q}_{z1}^K + C_{33}^K\mathbb{Q}_{x1}^K & C_{23}^K\mathbb{Q}_{z2}^K + C_{33}^K\mathbb{Q}_{x2}^K & C_{23}^K\mathbb{Q}_{z3}^K + C_{33}^K\mathbb{Q}_{x3}^K \end{bmatrix}.$$

The vector $\mathbb{S}^K$ is given by

$$\mathbb{S}^K = \left(0,\ 0,\ \mathbb{M}^K\underline{f}_{xx}^K,\ \mathbb{M}^K\underline{f}_{zz}^K,\ \mathbb{M}^K\underline{f}_{xz}^K\right)^T.$$

We consider now the discretization of the transmission condition (the last equation of (16)). The transmission condition on a face $F_j = \partial K^+ \cap \partial K^-$ such as $j = \beta(K^+, l) = \beta(K^-, g)$ is written as, $\forall \eta \in \mathbf{M}_h$

$$\int_F \left[\underline{\underline{\sigma}}_h^{K^+}\mathbf{n}^{K^+} \cdot \boldsymbol{\eta} + \underline{\underline{\sigma}}_h^{K^-}\mathbf{n}^{K^-} \cdot \boldsymbol{\eta} - \underline{\underline{S}}^{K^+}\left(\mathbf{v}_h^{K^+} - \lambda_h\right) \cdot \boldsymbol{\eta} - \underline{\underline{S}}^{K^-}\left(\mathbf{v}_h^{K^-} - \lambda_h\right) \cdot \boldsymbol{\eta}\right] = 0.$$

The corresponding discretization is given by the two following systems

$$\begin{aligned} &\mathbb{Q}_{xl}^{K^+{}^T}\underline{\sigma}_{xx}^{K^+} + \mathbb{Q}_{zl}^{K^+{}^T}\underline{\sigma}_{xz}^{K^+} - \tau^{(K^+,l)}\mathbb{F}_l^{K^+{}^T}\underline{v}_x^{K^+} + \tau^{(K^+,l)}\mathbb{G}^j\underline{\lambda}_x^{\beta(K^+,l)} \\ &\quad + \mathbb{Q}_{xl}^{K^-{}^T}\underline{\sigma}_{xx}^{K^-} + \mathbb{Q}_{zl}^{K^-{}^T}\underline{\sigma}_{xz}^{K^-} - \tau^{(K^-,l)}\mathbb{F}_l^{K^-{}^T}\underline{v}_x^{K^-} + \tau^{(K^-,l)}\mathbb{G}^j\underline{\lambda}_x^{\beta(K^-,l)} = 0, \end{aligned} \tag{B.8}$$

and

$$\begin{aligned} &\mathbb{Q}_{xl}^{K^+{}^T}\underline{\sigma}_{xz}^{K^+} + \mathbb{Q}_{zl}^{K^+{}^T}\underline{\sigma}_{zz}^{K^+} - \tau^{(K^+,l)}\mathbb{F}_l^{K^+{}^T}\underline{v}_z^{K^+} + \tau^{(K^+,l)}\mathbb{G}^j\underline{\lambda}_z^{\beta(K^+,l)} \\ &\quad + \mathbb{Q}_{xl}^{K^-{}^T}\underline{\sigma}_{xz}^{K^-} + \mathbb{Q}_{zl}^{K^-{}^T}\underline{\sigma}_{xz}^{K^-} - \tau^{(K^-,l)}\mathbb{F}_l^{K^-{}^T}\underline{v}_z^{K^-} + \tau^{(K^-,l)}\mathbb{G}^j\underline{\lambda}_z^{\beta(K^-,l)} = 0, \end{aligned} \tag{B.9}$$

where

$$\mathbb{G}_{im}^j = \int_{F_j} \psi_i\psi_m ds.$$

From (B.8) and (B.9) we write a local system for $\boldsymbol{\lambda}_h$

$$\mathbb{B}^K\underline{W}^K + \mathbb{L}^K\underline{\Lambda}^K + \mathcal{R}^K = 0, \tag{B.10}$$

where

$$\mathbb{B}^K = \begin{bmatrix} \mathbb{B}_{11}^K & \mathbb{B}_{12}^K \\ \mathbb{B}_{21}^K & \mathbb{B}_{22}^K \end{bmatrix},$$

$$\text{with} \quad \mathbb{B}_{11}^K = \begin{bmatrix} -\tau^{(K,1)}\mathbb{F}_1^{K^T} & 0 \\ -\tau^{(K,2)}\mathbb{F}_2^{K^T} & 0 \\ -\tau^{(K,3)}\mathbb{F}_3^{K^T} & 0 \end{bmatrix}, \; \mathbb{B}_{21}^K = \begin{bmatrix} 0 & -\tau^{(K,1)}\mathbb{F}_1^{K^T} \\ 0 & -\tau^{(K,2)}\mathbb{F}_2^{K^T} \\ 0 & -\tau^{(K,3)}\mathbb{F}_3^{K^T} \end{bmatrix},$$

$$\mathbb{B}_{12}^K = \begin{bmatrix} \mathbb{Q}_{x1}^{K^T} & 0 & \mathbb{Q}_{z1}^{K^T} \\ \mathbb{Q}_{x2}^{K^T} & 0 & \mathbb{Q}_{z2}^{K^T} \\ \mathbb{Q}_{x3}^{K^T} & 0 & \mathbb{Q}_{z3}^{K^T} \end{bmatrix}, \; \mathbb{B}_{22}^K = \begin{bmatrix} 0 & \mathbb{Q}_{z1}^{K^T} & \mathbb{Q}_{x1}^{K^T} \\ 0 & \mathbb{Q}_{z2}^{K^T} & \mathbb{Q}_{x2}^{K^T} \\ 0 & \mathbb{Q}_{z3}^{K^T} & \mathbb{Q}_{x3}^{K^T} \end{bmatrix},$$

$$\mathbb{L}^K = \text{Diag}\left(\mathbb{L}_{ii}^K\right),$$

with

$$\mathbb{L}_{ii}^K = \begin{cases} \tau^{(K,i)}\mathbb{G}^{\beta(K,i)}, & \text{for } i = 1,2,3, \\ \tau^{(K,i-3)}\mathbb{G}^{\beta(K,i-3)}, & \text{for } i = 4,5,6, \end{cases}$$

and $\mathcal{R}^K$ which gathers the contributions from the neighboring elements.

B2 Boundary conditions

In the previous section, we have considered that there is no boundary face. But for a correct implementation, we have to consider boundary faces and their discretization. The expression of the boundary conditions (3), (5) and (4) that we are considering: a free surface condition over Γ_l, $\quad \underline{\underline{\sigma}}\mathbf{n} = 0$; an absorbing boundary condition (ABC) over Γ_a, $\quad \underline{\underline{\sigma}}\mathbf{n} + \mathbf{PA}(\theta')\mathbf{P}^T\mathbf{v} = 0$. The boundary conditions are taken into account in the last equation of the global formulation (16) and modify the expression of the transmission condition. Using the notation $\mathbb{D}$ for the matrix $\mathbf{PA}(\theta')\mathbf{P}^T$, we can write a general formulation for both the isotropic and anisotropic cases

$$\begin{aligned} \int_F \left(\widehat{\underline{\underline{\sigma}}}_h \mathbf{n}\right) \cdot \boldsymbol{\eta} &= 0, && \text{for } F \in \mathcal{F}_h \backslash \mathcal{F}_b \\ \int_F \left(\widehat{\underline{\underline{\sigma}}}_h \mathbf{n}\right) \cdot \boldsymbol{\eta} &= \int_F \boldsymbol{g_l} \cdot \boldsymbol{\eta}, && \text{for } F \in \mathcal{F}_l \\ \int_F \left(\widehat{\underline{\underline{\sigma}}}_h \mathbf{n}\right) \cdot \boldsymbol{\eta} &= \int_F \boldsymbol{g_a} \cdot \boldsymbol{\eta}, && \text{for } F \in \mathcal{F}_a \end{aligned} \tag{B.11}$$

where g_l is the value that we impose on the Dirichlet boundary, we assume here that $g_l = 0$; and g_a is the value that we impose on the absorbing boundary, we assume here that $g_a = -\left(\mathbb{D}\boldsymbol{\lambda}_h\right)$. Replacing

$\widehat{\underline{\underline{\sigma}}}_h \mathbf{n}$ by the expression (15), we obtain

$$\begin{aligned} &\int_F [\![\underline{\underline{\sigma}}_h]\!] \cdot \boldsymbol{\eta} - \int_F 2\underline{\underline{S}} \left(\{\mathbf{v}_h\} - \boldsymbol{\lambda}_h\right) \cdot \boldsymbol{\eta} = 0, && \text{for } F \in \mathcal{F}_h \backslash \mathcal{F}_a \\ &\int_F [\![\underline{\underline{\sigma}}_h]\!] \cdot \boldsymbol{\eta} - \int_F 2\underline{\underline{S}} \left(\{\mathbf{v}_h\} - \boldsymbol{\lambda}_h\right) \cdot \boldsymbol{\eta} + \int_F (\mathbb{D}\boldsymbol{\lambda}_h) \cdot \boldsymbol{\eta} = 0, && \text{for } F \in \mathcal{F}_a \end{aligned} \tag{B.12}$$

Now, taking into account the boundary conditions in the transmission condition, the HDG formulation reads as, find $(\mathbf{v}_h, \underline{\underline{\sigma}}_h, \boldsymbol{\lambda}_h) \in \mathbf{V}_h^p \times \boldsymbol{\Sigma}_h^p \times \mathbf{M}_h$ such that $\forall K \in \mathcal{T}_h$, $\forall F \in \mathcal{F}_h$ and $\forall (\mathbf{w}, \underline{\underline{\xi}}, \boldsymbol{\eta}) \in \mathbf{V}^p(K) \times \boldsymbol{\Sigma}^p(K) \times \mathbf{M}^p(F)$

$$\left\{ \begin{array}{ll} \displaystyle\int_K i\omega\rho_K \mathbf{v}_h \cdot \mathbf{w} - \int_K \left(\nabla \cdot \underline{\underline{\sigma}}_h\right) \cdot \mathbf{w} + \int_{\partial K} \underline{\underline{S}} \left(\mathbf{v}_h - \boldsymbol{\lambda}_h\right) \cdot \mathbf{w} = 0, & \\ \displaystyle\int_K i\omega \underline{\underline{\sigma}}_h : \underline{\underline{\xi}} + \int_K \mathbf{v}_h \cdot \left(\boldsymbol{div}\left(\underline{\underline{C}}_K \underline{\underline{\xi}}\right)\right) - \int_{\partial K} \boldsymbol{\lambda}_h \cdot \left(\underline{\underline{C}}_K \underline{\underline{\xi}} \mathbf{n}\right) = \int_K \underline{\underline{\mathbf{f}}} : \underline{\underline{\xi}}, & \\ \displaystyle\int_F [\![\underline{\underline{\sigma}}_h]\!] \cdot \boldsymbol{\eta} - \int_F 2\underline{\underline{S}} \left(\{\mathbf{v}_h\} - \boldsymbol{\lambda}_h\right) \cdot \boldsymbol{\eta} = 0, & \text{if } F \in \mathcal{F}_h \backslash \mathcal{F}_a \\ \displaystyle\int_F [\![\underline{\underline{\sigma}}_h]\!] \cdot \boldsymbol{\eta} - \int_F 2\underline{\underline{S}} \left(\{\mathbf{v}_h\} - \boldsymbol{\lambda}_h\right) \cdot \boldsymbol{\eta} + \int_F (\mathbb{D}\boldsymbol{\lambda}_h) \cdot \boldsymbol{\eta} = 0, & \text{if } F \in \mathcal{F}_a. \end{array} \right. \tag{B.13}$$

The discretization of the last equation of (B.13) on the boundary Γ_a is

$$\begin{aligned} \mathbb{Q}_{xl}^K \underline{\sigma}_{xx}^K &+ \mathbb{Q}_{zl}^K \underline{\sigma}_{xz}^K - \tau^{(K,l)} \mathbb{F}_l^K \underline{v}_x^K + \tau^{(K,l)} \mathbb{G}^j \underline{\lambda}_x^{\beta(K,l)} \\ &+ D_{11} \mathbb{G}^F \underline{\lambda}_x^{\beta(k,l)} + D_{12} \mathbb{G}^F \underline{\lambda}_z^{\beta(k,l)} = 0, \end{aligned} \tag{B.14}$$

and

$$\begin{aligned} \mathbb{Q}_{xl}^K \underline{\sigma}_{xz}^K &+ \mathbb{Q}_{zl}^K \underline{\sigma}_{zz}^K - \tau^{(K,l)} \mathbb{F}_l^K \underline{v}_z^K + \tau^{(K,l)} \mathbb{G}^j \underline{\lambda}_z^{\beta(K,l)} \\ &+ D_{22} \mathbb{G}^F \underline{\lambda}_z^{\beta(k,l)} + D_{21} \mathbb{G}^F \underline{\lambda}_x^{\beta(k,l)} = 0. \end{aligned} \tag{B.15}$$

Remark 1. The expressions of the coefficients of the matrix $\mathbb{D}$ in the isotropic case are given by

$$D_{11} = -\rho \left(v_p^K n_x^{K^2} + v_s^K n_z^{K^2}\right),$$

$$D_{12} = D_{21} = -\rho n_x^K n_z^K \left(v_p^K - v_s^K\right),$$

$$D_{22} = -\rho \left(v_p^K n_z^{K^2} + v_s^K n_x^{K^2}\right).$$

For an element having a face on the absorbing boundary, the matrix $\mathbb{B}^K$ is not modified, whereas matrix $\mathbb{L}^K$ becomes, assuming without loss of generality that the absorbing edge is the edge $l = 1$ of

K,

$$\mathbb{L}^K = \begin{bmatrix} \zeta_1^K \mathbb{G}^{\beta(K,1)} & 0 & 0 & D_{12}\mathbb{G}^{\beta(K,1)} & 0 & 0 \\ 0 & \tau^{(K,2)}\mathbb{G}^{\beta(K,)} & 0 & 0 & 0 & 0 \\ 0 & 0 & \tau^{(K,3)}\mathbb{G}^{\beta(K,3)} & 0 & 0 & 0 \\ D_{21}\mathbb{G}^{\beta(K,1)} & 0 & 0 & \zeta_2^K \mathbb{G}^{\beta(K,1)} & 0 & 0 \\ 0 & 0 & 0 & 0 & \tau^{(K,2)}\mathbb{G}^{\beta(K,2)} & 0 \\ 0 & 0 & 0 & 0 & 0 & \tau^{(K,3)}\mathbb{G}^{\beta(K,3)} \end{bmatrix},$$

with $\zeta_1^K = \left(\tau^{(K,1)} + D_{11}\right)$ and $\zeta_2^K = \left(\tau^{(K,1)} + D_{22}\right)$.

B3 Construction of the global linear system

In the previous sections, we have shown that the HDG formulation requires the solution to

$$\mathbb{A}^K \underline{W}^K + \mathbb{C}^K \underline{\Lambda}^K = \mathbb{S}^K. \tag{B.16}$$

and

$$\mathbb{B}^K \underline{W}^K + \mathbb{L}^K \underline{\Lambda}^K + \mathcal{R}^K = 0, \tag{B.17}$$

where the boundary conditions are only included in the expression of the coefficients of the matrix $\mathbb{L}^K$. These two equations allow to obtain the local system element-by-element. As we use a Discontinuous Galerkin method, we have to assemble these local problems and to solve the global linear system. In order to obtain it, we denote by $N_\lambda^{(e,l)}$ the number of degrees of freedom of the l-th face of K_e, N_λ the total number of degrees of freedom of Λ and

$$\overline{N}_\lambda = \sum_{e=1}^{N_e} \sum_{l=1}^{3} N^{(e,l)}.$$

We thus define the trace space spreading operator $\mathcal{A}_{HDG}$ as a matrix of size $\overline{N}_\lambda \times N_\lambda$ which allows to map the unique global trace space values $\underline{\Lambda}$ onto their local values on each face of the element K, $\underline{\Lambda}^K$. We can organize $\mathcal{A}_{HDG}$ by elements such as

$$\mathcal{A}_{HDG} = \begin{pmatrix} \mathcal{A}_{HDG}^1 \\ \vdots \\ \mathcal{A}_{HDG}^{N_e} \end{pmatrix} \text{ and } \mathcal{A}_{HDG}^K \underline{\Lambda} = \underline{\Lambda}^K.$$

Then we rewrite (B.16) as

$$\mathbb{A}^K \underline{W}^K + \mathbb{C}^K \mathcal{A}_{HDG}^K \underline{\Lambda} = \mathbb{S}^K, \tag{B.18}$$

and consequently we can express $\underline{W}^K$ in terms of $\underline{\Lambda}$

$$\underline{W}^K = (\mathbb{A}^K)^{-1}\mathbb{S}^K - (\mathbb{A}^K)^{-1}\mathbb{C}^K\mathcal{A}_{HDG}^K\underline{\Lambda}. \tag{B.19}$$

By summing all the equations of the transmission condition on all the faces of each element, element by element, we obtain

$$\sum_{K\in\mathcal{T}_h}(\mathcal{A}_{HDG}^K)^T\left[\mathbb{B}^K\underline{W}^K + \mathbb{L}^K\mathcal{A}_{HDG}^K\underline{\Lambda}\right] = 0, \tag{B.20}$$

where the sum over all the elements along with the left application of the transpose of $\mathcal{A}_{HDG}^K$ allow to gather the element-wise contributions corresponding to faces. By replacing $\underline{W}^K$ in (B.20), we obtain a global system in $\underline{\Lambda}$,

$$\sum_{K\in\mathcal{T}_h}(\mathcal{A}_{HDG}^K)^T\left[\mathbb{B}^K(\mathbb{A}^K)^{-1}\mathbb{S}^K - \mathbb{B}^K(\mathbb{A}^K)^{-1}\mathbb{C}^K + \mathbb{L}^K\right]\mathcal{A}_{HDG}^K\underline{\Lambda} = 0, \tag{B.21}$$

and finally the HDG global linear system reads as

$$\sum_{K\in\mathcal{T}_h}(\mathcal{A}_{HDG}^K)^T\left[-\mathbb{B}^K(\mathbb{A}^K)^{-1}\mathbb{C}^K + \mathbb{L}^K\right]\mathcal{A}_{HDG}^K\underline{\Lambda} = \sum_{K\in\mathcal{T}_h} -(\mathcal{A}_{HDG}^K)^T\mathbb{B}^K(\mathbb{A}^K)^{-1}\mathbb{S}^K. \tag{B.22}$$

Remark 2. In the isotropic case, we obtain a global system similar to (B.22). The only difference between the isotropic case and the anisotropic case is in the expression of the matrices $\mathbb{A}^K$ and $\mathbb{C}^K$, which have a simpler expression.

Remark 3. The symmetry of the global matrix is not obvious but it can be easily demonstrated. The advantage of considering a symmetric formulation is the reduction of the memory usage when solving the linear system by a sparse direct solver based on a factorization method.

B4 Symmetry of the HDG formulation

In view of the expression of the local matrices $\mathbb{A}^K, \mathbb{B}^K, \mathbb{C}^K$ and $\mathbb{L}^K$, the global matrix of the HDG formulation (B.22) introduced previously seems to be not symmetric. However, by studying each local matrices, we can establish a symmetric formulation. Indeed, it is clear that the matrix $\mathbb{L}^K$ is a symmetric matrix since it is a diagonal matrix for a purely internal element K while, for an element K possessing at least one absorbing edge, we have $D_{12} = D_{21}$. The symmetry of the matrix $\left(\mathbb{B}^K(\mathbb{A}^K)^{-1}\mathbb{C}^K\right)$ is a little bit more complicated to determine. We remind that matrices $\mathbb{B}^K$ and $\mathbb{C}^K$ are written as

$$\mathbb{B}^K = \begin{bmatrix}\mathbb{B}_{11}^K & \mathbb{B}_{12}^K\\ \mathbb{B}_{21}^K & \mathbb{B}_{22}^K\end{bmatrix},\ \mathbb{C}^K = \begin{bmatrix}\mathbb{C}_{11}^K & \mathbb{C}_{12}^K\\ \mathbb{C}_{21}^K & \mathbb{C}_{22}^K\end{bmatrix},$$

and it is clear that

$$\mathbb{C}_{11}^K = \left(\mathbb{B}_{11}^K\right)^T \quad \text{and} \quad \mathbb{C}_{12}^K = \left(\mathbb{B}_{21}^K\right)^T.$$

We now define the matrix $\mathbb{T}^K$ by

$$\mathbb{T}^K = \begin{bmatrix} C_{11}^K \mathbb{I}^K & C_{12}^K \mathbb{I}^K & C_{13}^K \mathbb{I}^K \\ C_{12}^K \mathbb{I}^K & C_{22}^K \mathbb{I}^K & C_{23}^K \mathbb{I}^K \\ C_{13}^K \mathbb{I}^K & C_{23}^K \mathbb{I}^K & C_{33}^K \mathbb{I}^K \end{bmatrix},$$

where $\mathbb{I}^K$ is the identity matrix of size the number of lines of matrices $\mathbb{Q}_{jk}^K$, $j = x, z$ and $k = 1, 2, 3$, i.e. the number of degrees of freedom on the face k. By introducing the matrix $\mathbb{T}^K$, we remark that

$$\mathbb{C}_{21}^K = -\mathbb{T}^K \left(\mathbb{B}_{12}^K\right)^T \quad \text{and} \quad \mathbb{C}_{22}^K = -\mathbb{T}^K \left(\mathbb{B}_{22}^K\right)^T.$$

Hence, the matrix $\mathbb{C}^K$ can be expressed as follow

$$\mathbb{C}^K = \mathbb{N}^K \left(\mathbb{B}^K\right)^T,$$

with $\mathbb{N}^K = \begin{bmatrix} \mathbb{I}^K & 0 \\ 0 & -\mathbb{T}^K \end{bmatrix}$.

Now, we have to show that matrix $\left(\mathbb{A}^K\right)^{-1}$ is symmetric. From the expression of $\mathbb{A}^K$ given in section B, we observe that

$$\mathbb{A}_{21}^K = -\mathbb{T}'^K \mathbb{A}_{12}^{K^T},$$

with

$$\mathbb{T}'^K = \begin{bmatrix} C_{11}^K \mathbb{I}'^K & C_{12}^K \mathbb{I}'^K & C_{13}^K \mathbb{I}'^K \\ C_{12}^K \mathbb{I}'^K & C_{22}^K \mathbb{I}'^K & C_{23}^K \mathbb{I}'^K \\ C_{13}^K \mathbb{I}'^K & C_{23}^K \mathbb{I}'^K & C_{33}^K \mathbb{I}'^K \end{bmatrix},$$

where $\mathbb{I}'^K$ is the identity matrix of size equal to the one of $\mathbb{D}_j^K$. The matrix $\mathbb{T}'^K$ is a symmetric positive definite matrix, since $C^K \neq 0$ is symmetric positive definite. Thus we can write

$$\mathbb{A}^K = \begin{bmatrix} \mathbb{A}_{11}^K & \mathbb{A}_{12}^K \\ -\mathbb{T}'^K \mathbb{A}_{12}^{K^T} & -\mathbb{T}'^K \left(-\mathbb{T}'^K\right)^{-1} \mathbb{A}_{22} \end{bmatrix} = \mathbb{N}'^K \widetilde{\mathbb{A}^K},$$

with

$$\widetilde{\mathbb{A}^K} = \begin{bmatrix} \mathbb{A}_{11}^K & \mathbb{A}_{12}^K \\ \mathbb{A}_{12}^{K^T} & \left(-\mathbb{T}'^K\right)^{-1} \mathbb{A}_{22} \end{bmatrix} \text{ and } \mathbb{N}'^K = \begin{bmatrix} \mathbb{I}''^K & 0 \\ 0 & -\mathbb{T}'^K \end{bmatrix},$$

The matrix $\mathbb{I}''^K$ is the identity matrix of size than twice the size of the matrix $\mathbb{M}^K$. As the block $\left(-\mathbb{T}'^K\right)^{-1} \mathbb{A}_{22}$ is diagonal, the matrix $\widetilde{\mathbb{A}^K}$ is symmetric. In addition, we observe that

$$\mathbb{N}'^K = \mathbb{N}^{K^T} \mathbb{P},$$

where $\mathbb{P} = \begin{bmatrix} \mathbb{I}^{K^T} & 0 \\ 0 & \mathbb{I}^{K^T} \end{bmatrix}$. Finally, the matrix $\left(\mathbb{B}^K \left(\mathbb{A}^K\right)^{-1} \mathbb{C}^K\right)$ can be written as

$$\mathbb{B}^K \mathbb{N}^{K^T} \mathbb{P} \widetilde{\mathbb{A}^K} \mathbb{N}^K \mathbb{B}^{K^T},$$

and we deduce of this expression the symmetry of the global matrix of the HDG formulation. It is worth noting that, here, we do not want to express matrices $\mathbb{A}^K$ and $\mathbb{C}^K$ in another way but we want to demonstrate the symmetry of the global matrix by using another expression of the local matrices.

APPENDIX C: ALGORITHMS

We briefly describe here the algorithms of the different methods that we used for the performance comparisons. Classical DG methods and continuous finite element methods follow the same basic algorithm : (1) construction of the matrix and (2) solution of the associated linear system. The HDG method requires an additional step for the reconstruction of the solution once the Lagrange multiplier is computed.

C1 Upwind flux-based DG (UDG)

The upwind flux-based DG algorithm is constructed from the variational formulation (A.2), where the stabilization tensor is defined by using a technique similar to the one proposed in (El Bouajaji & Lanteri 2013) for electromagnetics. We refer the reader to (Bonnasse-Gahot 2015), chapter 2, for more details on the computation of this flux for elastodynamics. The upwind flux-based DG method yields a linear system $\mathbb{A}_{UDG}\underline{W} = \underline{F}_{UDG}$, where $\underline{W}$ is a global vector gathering the vectors $\underline{W}^K$ of the DG degrees of freedom of all the elements K, $\mathbb{A}_{UDG}$ is the matrix derived from the variational formulation and $\underline{F}_{UDG}$ is the vector associated to the source terms. The matrix is built using a loop over all the elements, and the linear system is solved thanks to MUMPS. Even if the particular flux we use leads to a symmetric matrix $\mathbb{A}_{UDG}$, the code has been built for more general fluxes and does not take advantage of the symmetry.

C2 IPDG algorithm

The IPDG algorithm is constructed from the second order variational formulation : find $\mathbf{v}_h \in \mathbf{V}_h^p$, such that $\forall K \in \mathcal{T}_h$, and $\forall \mathbf{w} \in \mathbf{V}^p(K)$

$$-\int_K \omega^2 \rho_K \mathbf{v}_h \cdot \mathbf{w} - a(\mathbf{v}_h, \mathbf{w}) = \int_K \mathbf{div}\, \underline{\underline{\mathbf{f}}} \cdot w, \tag{C.1}$$

where the bilinear form $a(\cdot,\cdot)$ is symmetric and coercive. We refer to (Rivière 2008) or (Barucq, Djellouli, & Estecahandy 2014b) for the expression of this bilinear form. We have slightly modified it

by incorporating the absorbing boundary condition proposed in (Barucq *et al.* 2014), which preserves its symmetry. This IPDG method yields a linear system $\mathbb{A}_{IPDG}\underline{V} = \underline{F}_{IPDG}$, where $\underline{V}$ is a global vector gathering the vectors $\underline{V}^K = (\underline{v}_x^K, \underline{v}_y^K)$ on all the elements K, $\mathbb{A}_{IPDG}$ is the symmetric matrix derived from the variational formulation and $\underline{F}_{IPDG}$ is the vector associated to the source terms. The matrix is built using a loop over all the elements, and the linear system is solved thanks to MUMPS. An option in the code allows for taking advantage of the symmetry of $\mathbb{A}_{IPDG}$ by storing only the upper part and by using the symmetric option of MUMPS (by setting the MUMPS parameter SYM to 2).

Compared with UDG, the IPDG algorithm allows to invert a linear system involving only the components of the velocity field. If needed, the stress components can be obtained after the inversion as a post-processing step. Therefore, for a given mesh, IPDG is always computationally cheaper that UDG for a similar accuracy.

C3 Continuous Galerkin (CG) algorithm

The variational formulation associated to the CG algorithm is similar to (C.1), except that the unknowns and the test functions belong to a continuous finite element space. Hence, CG also yields a linear system $\mathbb{A}_{CG}\tilde{\underline{V}} = \underline{F}_{CG}$, with a symmetric matrix $\mathbb{A}_{CG}$ and a vector $\tilde{\underline{V}}$ gathering the unknowns at the continuous Lagrange degrees of freedom. As for IPDG, an option in the code allows for taking advantage of the symmetry of $\mathbb{A}_{IPDG}$ by storing only the upper part, using the appropriate option of MUMPS (by setting the MUMPS parameter SYM to 2).

C4 HDG algorithm

From the implementation point of view, the HDG method differs from a classical DG method, although the main phases are similar: construction of the global linear system (algorithm 1), construction of the right-hand side (algorithm 2) and linear system solution (algorithm 3). One of the main differences in the implementation is that in a classical DG method, we only have to deal with volumic degrees of freedom which are local to mesh elements, while in the HDG method we also have to deal with the degrees of freedom of the hybrid variable, which are global and associated to mesh faces. Thus, the implementation of a HDG method is a mix between that of a DG method (local volumic degrees of freedom) and that of a CG method (global degrees of freedom). Another important distinction stems from the reconstruction step, which is specific to HDG methods. Since the local matrices involved in this step are also used for the construction of the global matrix, we have two possibilities: (1) to store all the local matrices during the construction step or (2) to recompute them during the reconstruction phase. We have chosen here the first option, which represents an increase in the memory usage by

about 7% to 27%, depending on the size of the problem. For larger problems, it is probably wiser to recompute these matrices. In such a case, the increase of the computational cost will be negligible since the reconstruction phase is highly parallelizable. By choosing strategy (1), we cannot evaluate precisely the computational time required for the reconstruction. However, we can get an upper bound of this cost by computing the computational time of the construction phase.

Algorithm 1 Construction of the linear system for the hybrid variable unknowns.

for $K = 1$ to Nb_{tri} **do**
  Compute local mass matrix $\mathbb{M}^K$ and stiffness matrices $\mathcal{D}_u^K$, with $u = x, z$
  for $l = 1$ to 3 **do**
    Compute matrices $\mathbb{E}_l^K,\ \mathbb{F}_l^K,\ \mathbb{Q}_{ul}$, with $u = x, z$, and $\mathbb{G}^{j=\beta(K,l)}$
  end for
  Compute matrices $\mathbb{A}^K$, $\mathbb{B}^K$, $\mathbb{C}^K$ and $(\mathbb{A}^K)^{-1}\mathbb{C}^K$.
  Compute matrix $\mathbb{L}^K$ taking into account the boundary conditions if necessary.
  Compute $\mathbb{K}^K = \mathbb{B}^K(\mathbb{A}^K)^{-1}\mathbb{C}^K + \mathbb{L}^K$
  Apply operator $\mathcal{A}_{HDG}^K$ for connecting local and global degrees of freedom
  Assemble the corresponding section in the global matrix $\mathbb{K}$
end for

Algorithm 2 Construction of the right-hand side.

Localization of the point source S
for $K = 1$ to Nb_{tri} **do**
  Construct local matrices $\mathbb{S}^K$
  Compute $\mathbb{B}^K\mathbb{S}^K$
  Apply operator $\mathcal{A}_{HDG}^K$ for connecting local and global degrees of freedom
  Assemble the corresponding section into the global right-hand side $\mathbb{S}$
end for

Algorithm 3 Linear system solution for the hybrid variable unknowns.

Solve the linear system $\mathbb{K}\Lambda = \mathbb{S}$ using MUMPS
Compute the local solutions $\underline{W}^K$
for $K = 1$ to Nb_{tri} **do**
  Apply operator $\mathcal{A}_{HDG}^K$ for connecting local and global degrees of freedom
  Compute $\underline{W}^K = -(\mathbb{A}^K)^{-1}\mathbb{C}^K\mathcal{A}_{HDG}^K\underline{\Lambda} = -(\mathbb{A}^K)^{-1}\mathbb{C}^K\underline{\Lambda}^K$
end for